Monoclinal flexure of an orogenic plateau margin during subduction, south Turkey

Running title: Monoclinal flexure plateau margin

David Fernández-Blanco[1], Giovanni Bertotti[2], Ali Aksu[3] and Jeremy Hall[3]

[1]Tectonics and Structural Geology Department, Faculty of Earth and Life Sciences, Vrije Universiteit Amsterdam, De Boelelaan 1085, 1081 HV Amsterdam, the Netherlands geo.david.fernandez@gmail.com

[2]Department of Geotechnology, Faculty of Civil Engineering and Geosciences, Delft University of Technology, Stevinweg 1, 2628CN, Delft, the Netherlands

[3] Department of Earth Sciences, Centre for Earth Resources Research, Memorial University of Newfoundland, St. John's, Newfoundland, Canada A1B 3X5

Abstract

Geologic evidence across orogenic plateau margins helps to discriminate the relative contributions of orogenic, epeirogenic and/or climatic processes leading to growth and maintenance of orogenic plateaus. Here, we discuss the mode of formation of the southern margin of the Central Anatolian Plateau (SCAP) and evaluate its time of formation using fieldwork in the onshore and seismic reflection data in the offshore. In the onshore, uplifted Miocene rocks in a dip-slope topography show monocline flexure over >100 km, km-scale asymmetric folds verging south, and outcrop-scale syn-sedimentary reverse faults. On the Turkish shelf, vertical faults transect the basal latest Messinian of a ~10 km fold where on-structure syntectonic wedges and synsedimentary unconformities indicate pre-Pliocene uplift and erosion, followed by Pliocene and younger deformation. Collectively, Miocene rocks delineate a flexural monocline at plateau margin scale that is expressed along our on-offshore sections as a kink-band fold with a steep flank ~20–25 km long. In these reconstructed sections, we estimate a relative vertical displacement of ~3.8 km at rates of ~0.5 mm/y, and horizontal shortening values <1 %. We use this evidence together with our observations of shortening at outcrop, basin, plateau-margin and forearc-system scales to infer that the SCAP forms as a monoclinal flexure to accommodate deep-seated thickening and shortening since >5 Ma, and to contextualize the plateau margin as the forearc high of the Cyprus subduction system.

Keywords: orogenic plateau; Anatolian plateau; plateau margin; south Turkey; monocline; Mut Basin; Cilicia Basin

1. Introduction

Many mechanisms are proposed to explain the growth of orogenic plateaus and the long-term feedbacks between their geodynamic and/or climatic controls (e.g., Bird, 1979; Powell, 1986; Nelson *et al.*, 1996; Pope & Willett, 1998; Yin & Harrison, 2000; Tapponnier *et al.*, 2001; Şengör *et al.*, 2003; Sobel *et al.*, 2003; Rowley & Currie, 2006; Garcia-Castellanos, 2007; Ballato *et al.*, 2010; Biryol *et al.*, 2011). While tectono-structural and thermo-mechanical models relate plateau margin growth to accretion/removal of crustal or lithospheric material, magmatic/tectonic underplating or rheological changes (e.g., Allmendinger *et al.*, 1997; Clark, 2012), the climatic-erodibility models relate the tectonic activity to climate, rock erodibility, and precipitation power during incipient relief development (e.g., Mulch *et al.*, 2006; Strecker *et al.*, 2009). Geologic data across plateau margins (on- and offshore) is pivotal to understand plateau margin growth and explain certain features that are not always entirely captured by these models.

Current studies advocate for epeirogenic causes to explain the growth and uplift of the Central Anatolian Plateau southern margin (SCAP) (e.g., Schildgen *et al.*, 2014). Shallow slab break-off and asthenospheric mantle upwelling are proposed as engines for the post-8 Ma surface uplift of the modern Central Taurides, occurring either separately from (Cosentino *et al.*, 2012), or jointly with, a second uplift phase, with rates of 0.6-0.7 mm/yr and leading to ~1200 m of topography, after ~1.6 Ma (Schildgen *et al.*, 2012), and a new uplift phase, with rates of 3.21-3.42 mm/yr and leading to up to 1500 m of topography, since ~450 ka (Öğretmen *et al.*, 2018). For these studies, the Central Taurides surface uplift is "passive" and detached from regional compression due to subduction (e.g., Schildgen *et al.*, 2014).

Epeirogenic models of plateau uplift that might apply in the Central Anatolia Plateau

interior (e.g., Bartol & Govers, 2014; Göğüş *et al.*, 2017) are at variance with geologic evidence farther south. For example, the Cyprus slab is imaged by tomography along the Central Cyprus subduction zone and below the modern Central Taurides (e.g., Bakırcı *et al.*, 2012; Abgarmi *et al.*, 2017), where a thick crust and mantle lithosphere exist (e.g., Delph *et al.,* 2017; Portner *et al.,* 2018). Also, the concomitance of uplift in the modern Central Taurides and subsidence in the offshore Outer Cilicia Basin (OCB) to the south (e.g., Walsh-Kennedy *et al.*, 2014) indicate short-wavelength vertical motions in the long-term, at odds with the long-wavelength vertical motions expected during asthenospheric upwelling (e.g., Göğüş & Pysklywec, 2008). Stable isotope paleoaltimetry estimates suggest that ~2 km of relief existed at ~5 Ma (Meijers *et al.*, 2018), a finding also at odds with models proposing epeirogenic uplift. Finally, compressional tectonics of the Cyprian subduction zone is attested by tapering-southward forearc basins atop south-verging thrust systems in the offshore (e.g., Aksu *et al.*, 2005a, 2005b; Calon *et al.*, 2005a, 2005b; Hall *et al.*, 2005a, 2005b), in the Kyrenia Range, and in the Messaoria Basin (e.g., McCay, 2010; McCay & Robertson, 2012; McCay *et al.*, 2012). These observations provide a different frame whereby the southern margin of the Central Anatolian Plateau may have been uplifted "actively" by contraction within the Cyprus subduction system.

Here, we apply a multi-scale approach and consider the SCAP within the larger context of subduction in the Central Cyprus Arc. We analyse key fieldwork observations in the Mut Basin, lying atop the Tauride Mountains to the north, and interpret and depth-convert N-S trending seismic lines in the offshore Outer Cilicia Basin (OCB) (Fig. 1). We link these basins in regional onshore-offshore cross-sections to delineate a monocline at plateau margin scale that we analyse geometrically. Integrating this with our data along the Central Cyprus forearc, we evaluate the time of formation of the plateau margin, and discuss its growth mechanism, tectonic setting and potential geodynamic drivers.

Figure 1. Location map, showing the main marine Miocene basins in and around the study area of this contribution (onshore basins are in yellow, offshore basins are marked by their acronyms). The structures depicted in this map are based on the analysis of 1-arc DEM and LandSat 7 images from NASA. We depict the motion of the structures as known in the available literature.

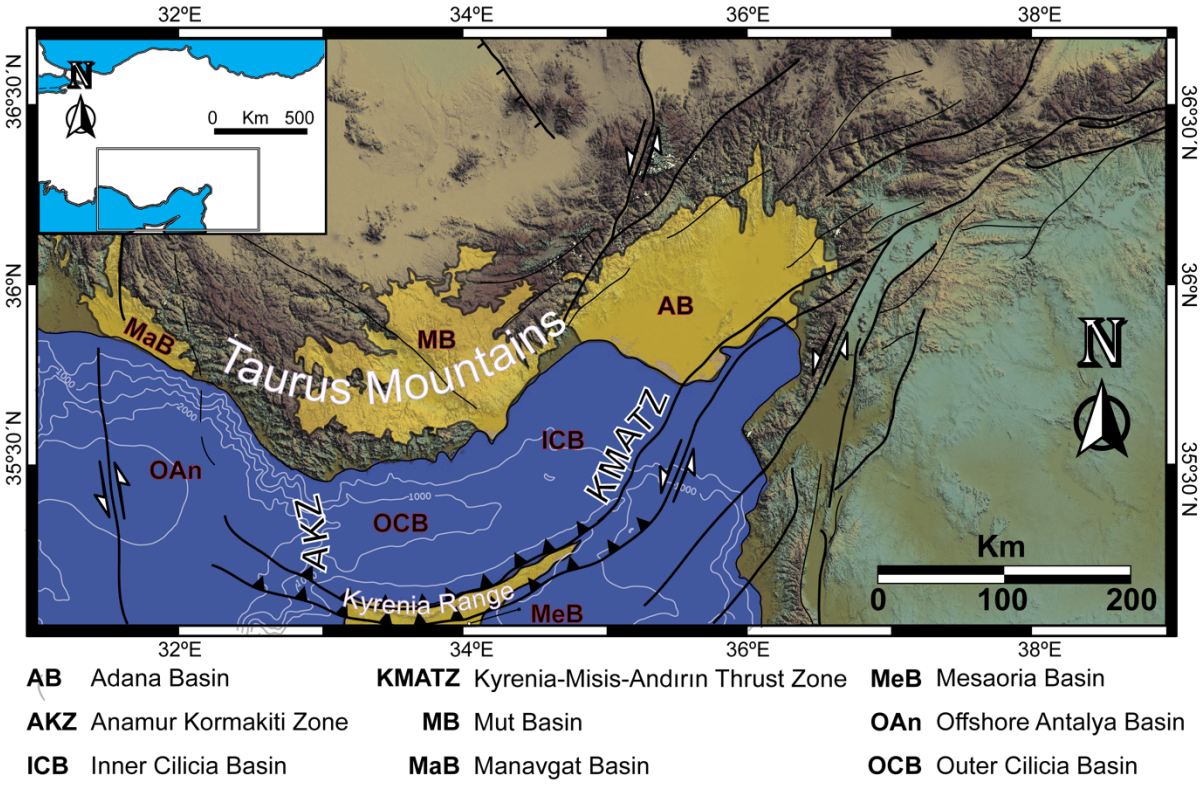

2. Background

A broad Miocene subsidence initiated marine deposition and led to a wide basin in the NE Mediterranean (e.g., Walsh-Kennedy *et al.*, 2014). This regional event allows for regional correlations across onshore and offshore sites in our region of study (Fig. 2). Whereas subsidence continued until present in the Cilicia Basin (in the centre of the marine basin), the basin was disrupted by uplift in the Central Taurides (to the north) (e.g., Cosentino et al., 2012), in the Kyrenia Range and to the south (e.g., Calon *et al.*, 2005a) (Fig. 3). Such vertical motions exceed glacio-eustatic signals described for the

area (e.g., Bassant *et al.*, 2005; Janson *et al.*, 2010; Cipollari *et al.*, 2013) and should be regarded as portraying two different tectonic events, i.e. protracted regional subsidence since the Early Miocene, and Late Miocene differential motions (Fig. 3).

Figure 2. Seismic stratigraphy of the Cilicia Basin, showing the correlations between seismic stratigraphic units and the onland sedimentary successions and exploration wells. Modified following Aksu et al. (2005a) and Calon et al. (2005b), and updated after Cosentino et al. (2013), Faranda et al., (2013).

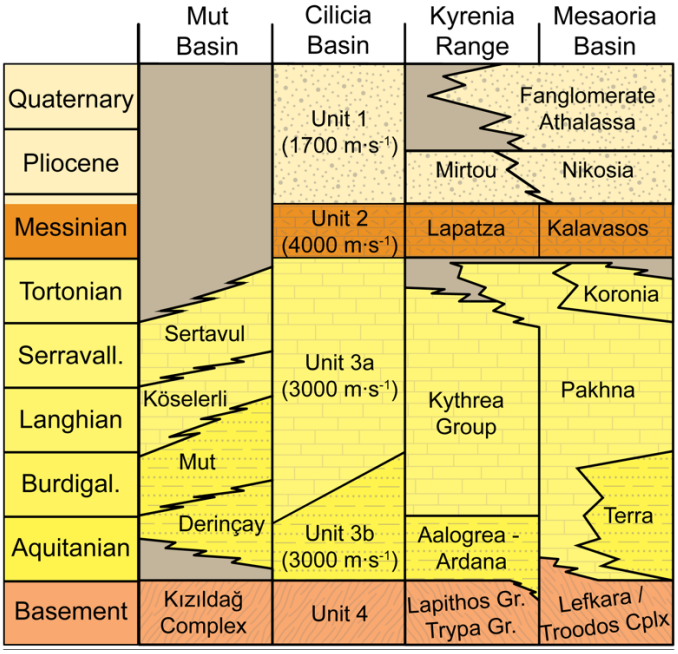

Figure 3. Schematic section showing first order vertical motions along the study area and their overall scale. The vertical scale is estimated as an approximation to the depth of deposition. The black line represents the position of the basement at every time-step, and the green area shows the location of the basement in the previous time-step. Arrows depict the relative vertical displacement between previous and succeeding time-steps. At the bottom, a schematic N-S regional cross section across study area (approx. from Karaman to Nicosia), shows the main type of depositional environment. Vertical exagg. ≈2.5.

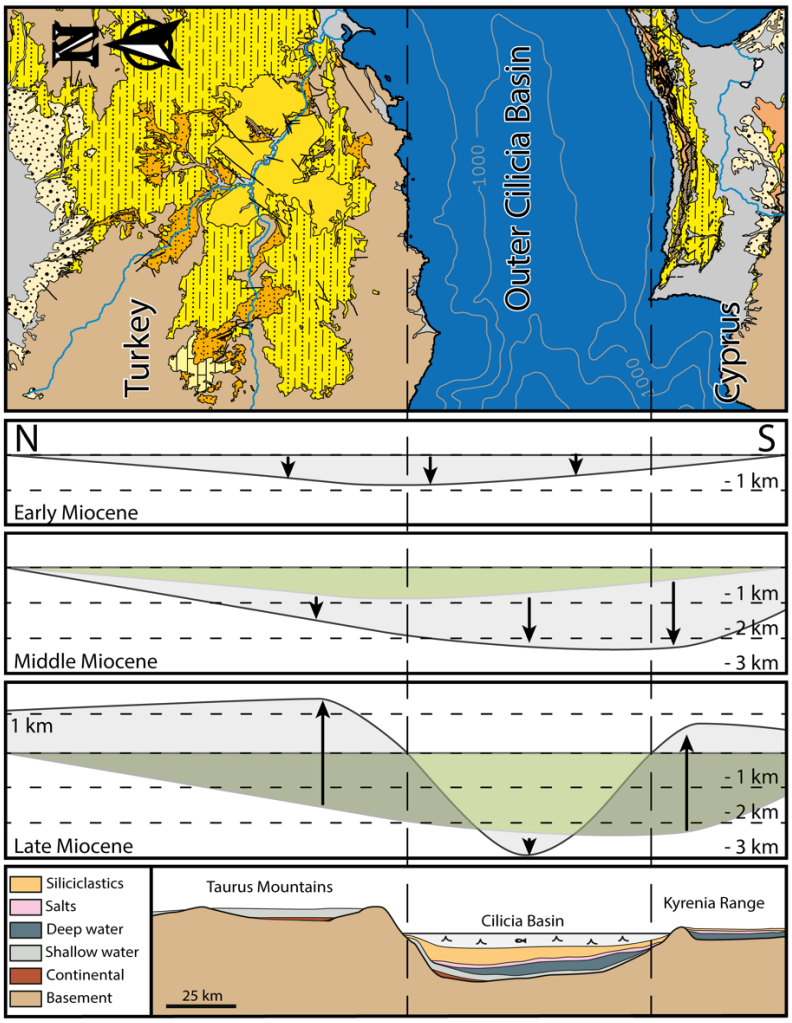

The broad subsidence changed Late Oligocene-Early Miocene continental deposition in Anatolia and surrounding regions (e.g., Yetiş *et al.*, 1995; Clark & Robertson, 2002, 2005) to marine deposition (e.g., Robertson, 1998; Bassant *et al.*, 2005; Eriş *et al.*, 2005; Şafak *et al.*, 2005). Continued subsidence resulted in a broad marine basin (e.g., Walsh-Kennedy *et al.*, 2014) that covered south Turkey (Karabıyıkoğlu *et al.*, 2000; Çıner *et al.*, 2008) (Fig. 1) and an extensive area further south (Aksu *et al.*, 2005a, 2005b; Burton-Ferguson *et al.*, 2005; Hall *et al.*, 2005a; Işler *et al.*, 2005). In the vicinity of the Kyrenia Range, deposition of the mostly deep-water upper Oligocene to upper Miocene sequence preceded shallow deposits, broadly similar to basins to the north and north-east, and with a common Tauride source (McCay & Robertson, 2012).

Surface uplift to the north exposes a sedimentary sequence of >1 km (Şafak et al., 2005) of the preceding Miocene basin on top of the Central Taurides. The top of this sequence is uplifted by 2 km and dated as ~8 Ma, Late Tortonian (Cosentino *et al.*, 2012), whereas younger rocks outcrop in paleo-valleys and areas near the coast (Öğretmen *et al.*, 2018). In the offshore to the south, the base of the Messinian reaches ~2 km depth in the Outer Cilicia Basin (OCB) (Aksu *et al.*, 2005a). Farther south, sedimentary deposits belonging to the preceding Miocene basin now outcrop in the Kyrenia Ridge (Calon *et al.*, 2005b; McCay *et al.*, 2012) (Fig. 3). While south-verging contractional structures accommodate these motions in the Kyrenia Range and further south, no regional upper-crustal structures are known to accommodate uplift in the Central Taurides.

2.1 Northern onshore domain: Central Taurides and Mut Basin

The E-W south-arched Central Taurides outcrop in the northern onshore domain, to the north of the OCB (Fig. 1). Lower to Upper Miocene sediments, mostly marine, were deposited atop the pre-Miocene Tauride basement (e.g., Monod, 1977; Andrew & Robertson, 2002; Bassant *et al.*, 2005; Eriş *et al.*, 2005) and then uplifted (Fig. 3). These marine sediments belong to the Mut Basin and are coeval with fluvio-lacustrine deposits known from seismics for the Tuz Gölü area farther north (Gorur *et al.*, 1984; Huvaz, 2009; Fernández-Blanco *et al.*, 2013). Rocks in both areas are in turn unconformably covered by terrace and alluvial fan Pliocene to Quaternary continental deposits (Monod *et al.*, 2006; Özsayin *et al.*, 2013) (Fig. 4 - section A). Miocene rocks in the southern margin of the Mut Basin may shape a monocline on top of the basement, with a roughly flat surface in the hinterland that progresses into gently south-dipping geometries in its southward offshore continuation (Fig. 4 B; Fig. 22 in Çıner et al., 2008). Regional upwarp flexure at

the scale of the Central Taurides cannot be accommodated by syn-depositional faulting leading to small-scale intrabasinal ridges and depressions (e.g., Ilgar & Nemec, 2005).

Figure 4. Map showing the different tectono-stratigraphic components in and around the study area. The geological map of South Turkey and Center-North Cyprus depicts a common age nomenclature for the Cenozoic units. The age integration is based on the ages shown for the MTA Geologic Map of Turkey 1:500.000, the Geological Map of Cyprus 1:250.000, and the stratigraphic correlation shown in Fig. 4. The map shows also the location of some figures of this contribution. On the right hand, the main geometric and contact relationships for the area and one representative study for each of them are shown.

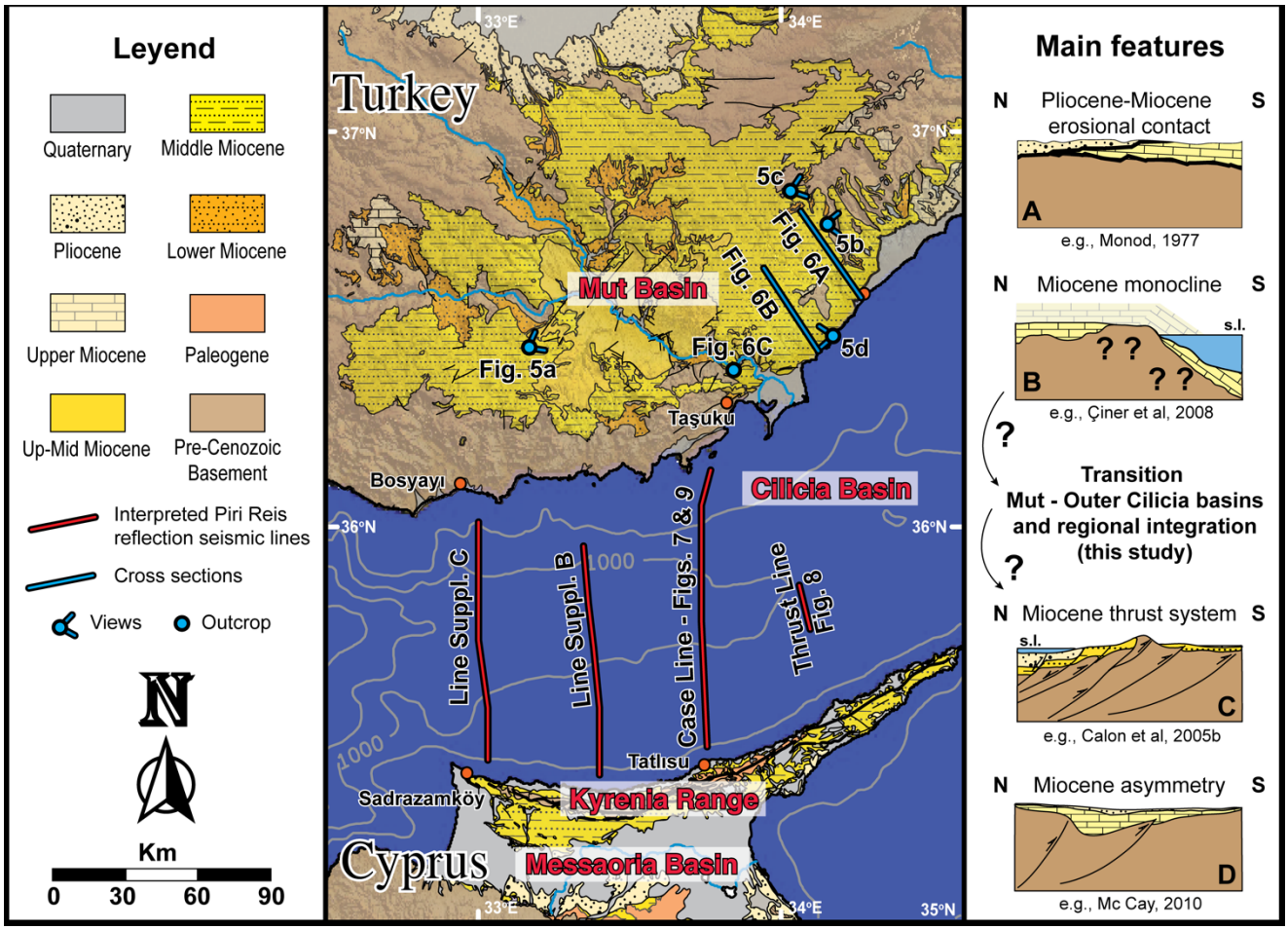

2.2 Offshore domain: Outer Cilicia Basin

The Outer Cilicia Basin (OCB) lies in the offshore domain between the mainland areas of south Turkey and north Cyprus (Figs. 1 & 4). The OCB is an ~160 km E-W elongated basin with a N-S extent of ca. 120 km (Fig. 1). The OCB sea floor has a concave shape that opens and deepens from 800 m to 1100 m westwards, and shallows gradually eastwards into the less in-filled basin sectors of Inner Cilicia and Adana (Evans *et al.*, 1978; Aksu *et al.*, 2005a). The Cilicia-Adana basin complex is bounded to the south and southeast by the arcuate culmination of the south-verging Kyrenia-Misis-Andırın Thrust Zone (Fig. 1). The culmination of these imbricate thrusts embays sediments with east and northeast sources (Evans *et al.*, 1978; McCay, 2010), and results in the asymmetrical deposition of thick Miocene and younger sediment infill of the basin complex (e.g., Aksu *et al.*, 2014), as well as its relatively flat and markedly shallow basin floor (Fig. 3). To the west, the OCB sea floor deepens ~1 km in a horizontal distance of ~50 km, towards the Antalya Basin.

2.3 Southern onshore domain: Kyrenia Range and Messaoria Basin

Bounding the OCB to the south is the E-W trending Kyrenia Range and further south, the Messaoria plain (Fig. 4). The Kyrenia Range outcrops as a deep-rooted imbricate thrust system that verges south (Calon *et al.*, 2005a, 2005b) setting basement and Miocene rocks atop Pliocene and being in turn covered by Pleistocene rocks (Calon *et al.*, 2005b; McCay & Robertson, 2012) (Fig. 4 - section C). Southwards, the Messaoria Basin is a wedge-top Paleocene to Recent asymmetric basin (McCay, 2010) (Fig. 4 - section D). Further south, focal mechanisms along the Cyprus Arc trench are compressional (Imprescia *et al.*, 2012).

3. Northern Onshore Domain: Central Taurides and Mut Basin

We conducted fieldwork in the Ermenek and Mut basins to study gently-deformed Miocene limestones of mostly shallow marine origin lying atop the modern Central Taurides. We aimed at: (i) determining the geometry of the basement-Miocene contact, (ii) identifying regional scale accommodation structures potentially contributing to the vertical movements, and (iii) assessing the regional stress field during the motions.

3.1 Monocline flexure in Miocene rocks

The Miocene rocks lie unconformably on, and in a parallel dip-slope to, the erosional surface that truncates the basement layers at high angles (Fig. 5-a,-b,-d). The Miocene succession overlies entirely pre-Miocene paleotopography of a few hundred metres (Fig. 5-a,-b), against which local onlaps are common (Fig. 5-c). When not eroded, the lateral continuity of the Miocene dip-slope is remarkable throughout the basin, implying that pre-Miocene paleotopography was fully covered by the Late Miocene. The Miocene dip-slope is best exposed in N-S and NW-SE steeply incised valleys, i.e. the Göksu River and rivers north of Erdemli (Fig. 5-a,-b). In the latter rivers, the Miocene marine succession can be followed for horizontal distances of ~20 km, losing elevation from ~1600 m to ~400 m (slopes of ~3%) (Fig. 5-b). While the succession gently gains elevation further north (Fig. 5-a), these rocks are often eroded in coastal areas southwards (Fig. 4).

The Miocene rocks form a monoclinal flexure at the scale of the entire basin (>100 km, Figs. 5-a). Along strike, the monocline has an arcuate geometry at the regional scale that follows to a large extent the modern coastline of south Turkey. The broad hinge of the monocline lies at ~40 km from the coast in the basin centre and ~30 km away from it eastwards. Across-strike, the inland limb is sub-horizontal, with overall dips ranging

from horizontal to 10° seaward, and transitions southwards to the steeper limb, with 8° to 20° dips seaward (Figs. 5-a). Regionally, dip angles of 10° dominate. Transitions both along and across the strike of the monocline are smooth. In brief, a regional-scale Miocene monoclinal flexure that dips gently southward transitions from the elevated topography of the Central Anatolian Plateau interior to the Mediterranean Sea (Fig. 5-a).

Figure 5. a) GoogleEarth oblique 3-D view of the Miocene monocline flexure at the scale of the whole Mut Basin, looking NE. The Göksu Gorge is in the middle-ground and the Cappadocia Volcanic Province and the Central Anatolian Plateau interior is in the background. b,-c,-d) Different views of the contact relationship between Miocene rocks atop basement rocks in the Mut Basin, roughly along latitude. Arrows mark the contact between the basement (below) and the infill (above). Basement-infill contact relationships are dependent on the scale of observation; deep-slope at the basin scale (b) yet locally onlapping (c).

David Fernández-Blanco et al., Figure 5, .ai

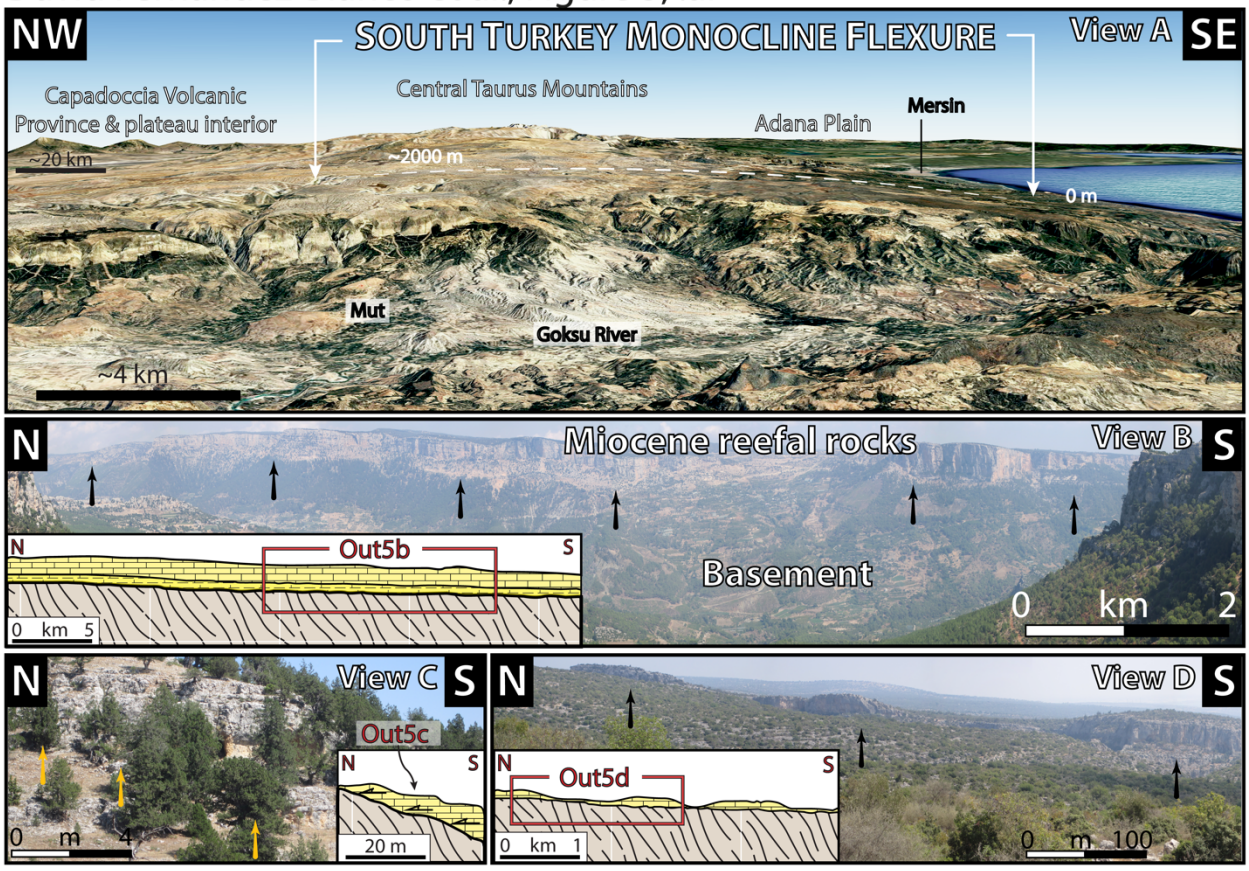

3.2 Other large-scale observations

Large-scale observations are consistent with regional contraction. Erosive terminations of the basin to east and west are parallel to basement ridges that outcrop in arched-south orientations parallel to the coast (ENE-WSW in the east of the Mut Basin, and E-W in the west) (Fig. 4 & 5). Miocene rocks predominantly strike parallel and dip perpendicular to the outcropping basement ridges they bound at present. This indicates that both pre-Miocene basement and Late Miocene rocks deform together after deposition of the Miocene rocks. Further, smaller folds with km-scale wavelengths form across-strike of the regional monocline. Folds are best observed to the SE of the Mut Basin along NW-SE geological cross-sections that run across the regional monocline axis and reach the coast (Fig. 6). Cross-sections in Fig. 6 have the best spatial coverage of bed attitude data of (Middle) Miocene immediately on top of the basement and depict the folds as gently asymmetrical with south-dipping flanks steeper than north-dipping ones. These observations agree with the regional monoclinal flexure of the modern Central Taurides.

3.3 Outcrop-scale observations

Syn-sedimentary outcrop-scale structures are scarce in the Miocene rocks of the Mut Basin. Figure 6 (bottom) shows several reverse faults in Middle Miocene limestones on a road-cut <10 km from the coast. Motion of internally coherent rock packages along faults with planar attitudes, resulting in fault-propagation fold “heads” at southerly positions, discounts formation by slumping in soft sediments. These reverse faults verge roughly to the SE and show striae on two fault planes that indicate a NW−SE motion (Fig. 6, bottom) and are immediately covered by inclined undeformed layers, thus characterising shortening during the Middle Miocene.

Figure 6. Cross-sections and reverse faults in the Mut Basin. The upper two panels show the geometries of the Miocene deposits and their relationships with basement. For each transect, the lower section corresponds to a 1:1 cross section representing the geometry of the first layer deposited on top of the basement, and the upper section represents a vertically exaggerated simplification of the Miocene and main geometries as well as representative field measurements. The depth of the basement is located on the basis of Bassant et al. (2005) and field observations. The lower panel shows reverse faults in a mid-Miocene outcrop. The upper image is a hand-drawn overview of the main structures seen in the outcrop and some representative in-place measurements. The lower image shows the interpretation drawn on top of a picture. On-site indications of relevant bed and fault attitude, and striae data are also shown.

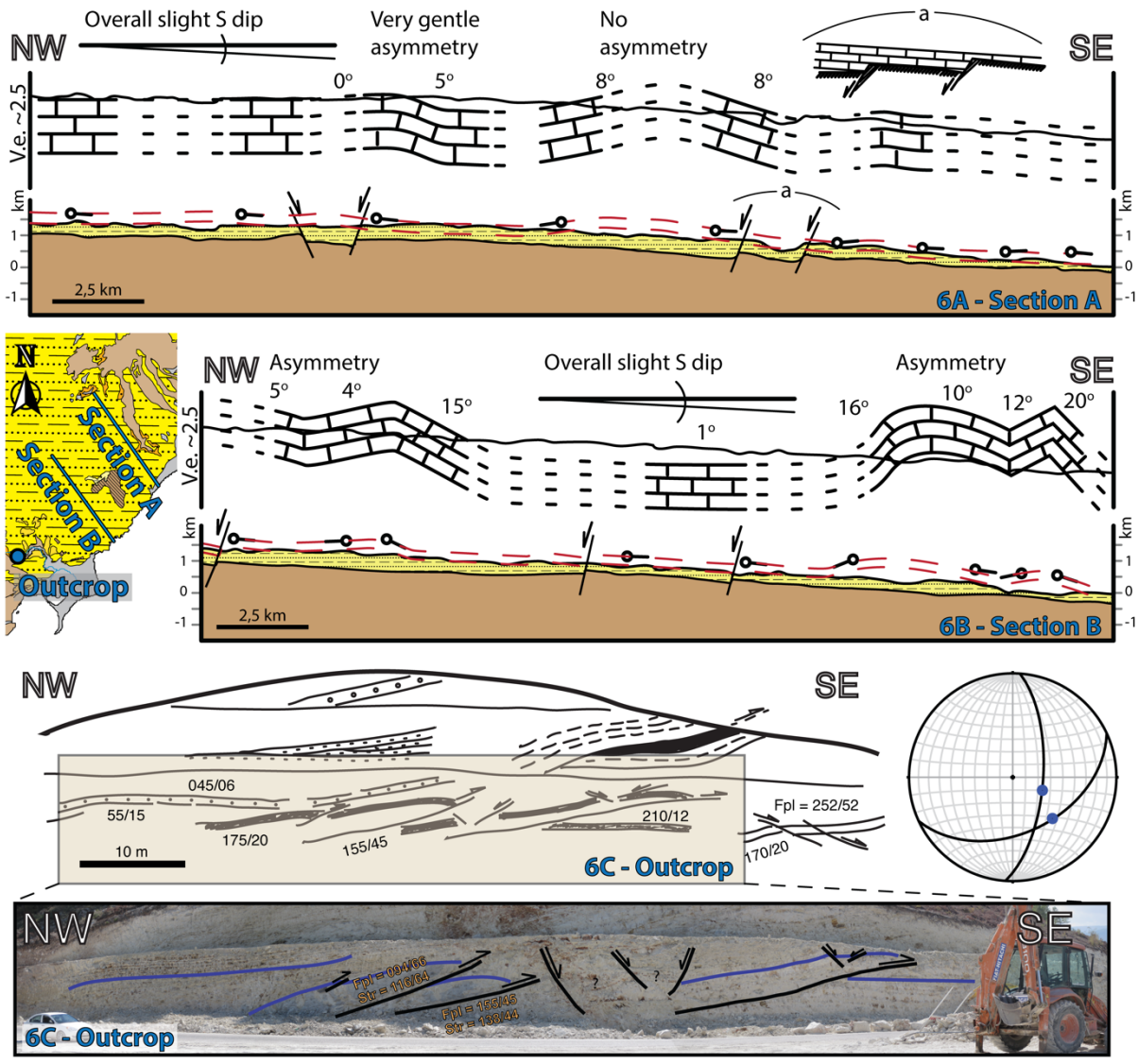

4. Offshore Domain: Outer Cilicia Basin

Seismic profiles in the area were obtained in 1991 and 1992 by the Memorial University of Newfoundland, in collaboration with the Institute of Marine Sciences and Technology, Dokuz Eylül University. We present here three N-S multichannel reflection profiles (Fig. 7 and Suppl. material B and C; location in Fig. 4), and an inset of a fourth line (Fig. 8). The three N-S seismic profiles, between 70 km and 100 km long, are ca. 30–35 km apart from each other in the east-west direction. Together, the seismic lines cover an area south of Turkish onland locations Bozyayı and Taşuku, and reach close to Sadrazamköy and Tatlısu towns on the Cyprus north coast (Fig. 4). We use the GeoSuite AllWorks® software to transform seismic profiles images in .pdf format to seismic data format (SEG-Y) and convert to true-depth to obtain the resulting interpreted seismic lines.

We use the regional correlation of Aksu et al., 2005a (see their Fig. 6) to constrain the age of the seismic units in the Cilicia-Adana basin complex, based on stratigraphic compilations from previous studies and bio-/lithostratigraphic data on exploration wells by the Turkish Petroleum Corporation (Aksu *et al.*, 2005a; Calon *et al.*, 2005b) (Fig. 1). This correlation is here updated on the basis of Cosentino *et al.* (2013) and Faranda *et al.* (2013) (Fig. 2). Suppl. A provides a succinct description of the seismic facies that are exhaustively described in Aksu *et al*. (2014).

We interpreted the seismic profiles by means of seismic facies. Characteristic packages of reflections allow the distinction of four seismo-stratigraphic units (second row in Figs. 7 & Suppl. B & C) that correspond to those originally defined by Aksu et al. (2005a) for the area. We traced the most continuous reflections in the depth-converted lines and analysed the modern geometry, unit thicknesses, contact relationships and syntectonic growth of all three seismic profiles (third row in Figs. 7 & Suppl. B & C). We

applied the seismic velocities in Fig. 2 to each seismic unit for time-to-depth conversion of the seismic profiles (fourth row in Figs. 7 & Suppl. B & C). All three seismic profiles are consistent laterally and show only limited variations across the OCB axis. Therefore, we describe below the eastern line and use it as representative for the OCB as a whole (Case Line; Fig. 7). We refer to the other two profiles (Suppl. B & C) in the text as needed.

Figure 7. Original, interpreted in two-way-traveltime (TWT), traced with reflections in TWT, and depth-converted profile Case Line.

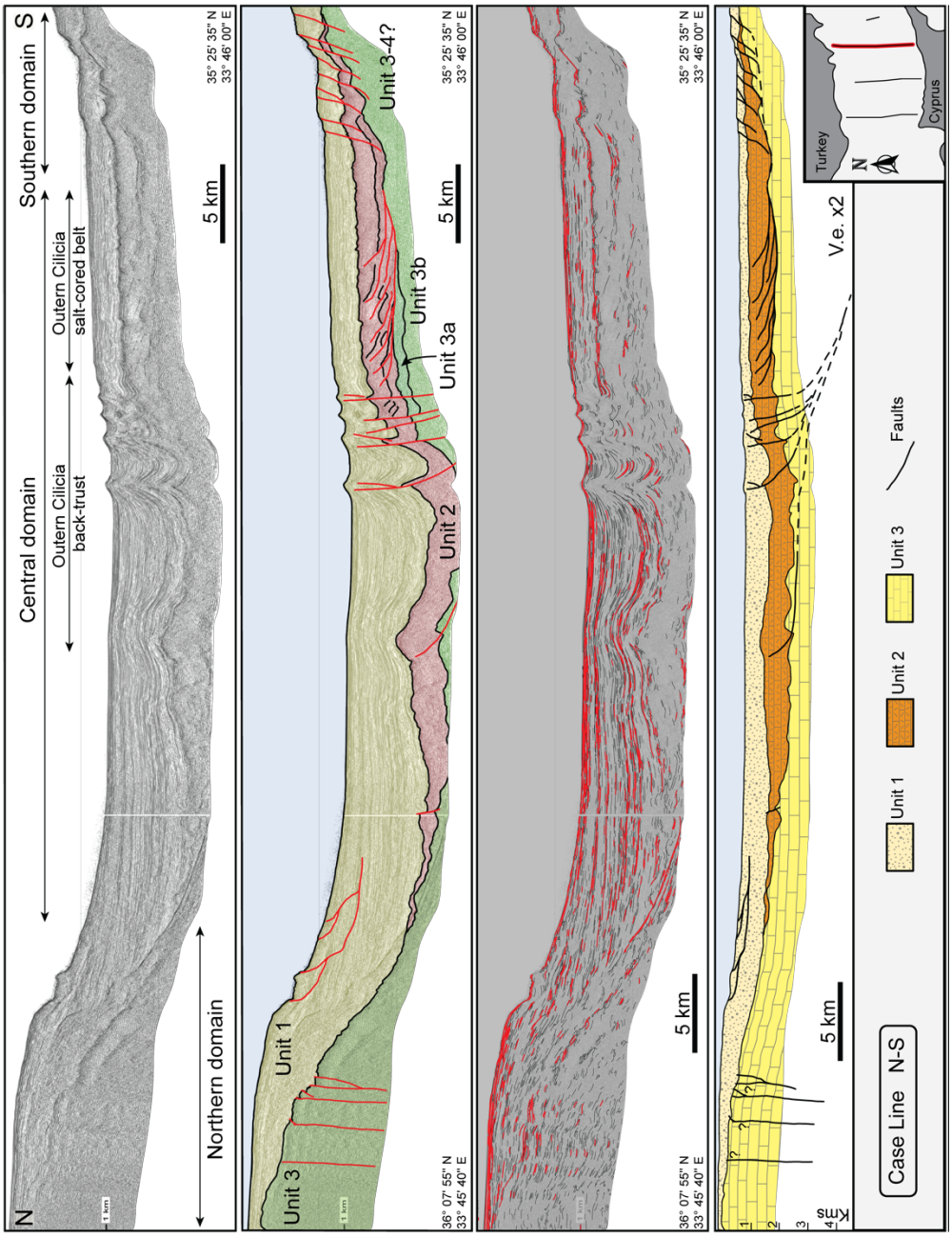

4.1 Contact relationships and thickness variations

In the northern end of the Case Seismic Line, the reflections of Unit 1 (latest Messinian - Recent) onlap the erosional surface bounding the pre-Messinian Miocene unit (Fig. 7). Southwards, Unit 1 reflections dip basinward and seismic packages show increasing thickness in this direction (from 200 m to 750 m in approx. 15 km). Immediately south of the Turkish shelf break, Unit 1 shows a broad depocentre (~25 km) with thicknesses of >850 m. Depocentre thicknesses are maximum to the north related to a series of S-dipping extensional faults that offset the sea floor and merge at a horizontal level ~1000 m below sea level. Thicknesses decrease to ca. 550 m within the central-southern area of the depocentre due to a pop-up structure in Unit 2 formed by a south-dipping thrust fault, leading to syntectonic wedging out of the Unit 1 reflections northward. To the south of the depocentre, Unit 1 thins to ~350 m and its base shallows in less than 5 km from depths of ~1900 m to 1200 m. Constant thicknesses of 300–350 m exist further south, except close to the continental shelf of north Cyprus, where Unit 1 thins, partially due to the extensional offsets of a north dipping fault system.

Unit 2 pinches out from the centre of the Case Seismic Line and shows a southward step-up sigmoidal shape, by which the same reflections are found at shallower positions to the south (Fig. 7). A prominent deep-rooted system of steep north-verging thrusts controls the sigmoidal shape of Unit 2 and the elevated position of the southern basin sector of the basin relative to the northern one. Immediately south of the steep deep-rooted thrusts, a smaller set of thrust faults dip gently southward. This second system is rooted in the base of Unit 2 and creates salt-cored anticlines that repeat the sequence and thicken Unit 2 up to maximum thicknesses of ~700–750 m. Unit 2 thins away from its depocentre both to the north and south in horizontal distances of <10 km.

Unit 3 has no evident terminations in the Case Line and its base cannot be distinguished and thus, no thickness determination was possible. At the northern end of the Case Line, an erosional unconformity below Unit 1 (latest Messinian- Recent) forms the top of Unit 3 (pre-Messinian Miocene) (Fig. 7). To the south, the unconformity fades and Unit 3 underlies the Messinian evaporites of Unit 2. Further south, the top surface of Unit 3 steps upward in the same direction and marks an offset in relation to the deep-rooted thrust system. At the southernmost end of the line, an erosional unconformity again sets the top of Unit 3.

4.2 Structural domains

A sea floor step divides the Outer Cilicia Basin (OCB) in two around its centre in relation to a deep-rooted thrust system observed in all seismic lines (Section 4.2.1; Figs. 7, 8, Suppl. B & C). Sea bottom depths are visibly shallower on the southern side than on the northern side of the basin, correlating with two structural domains trending E-W (Figs. 7, 8, Suppl. B & C), the northern (Section 4.2.2) and southern sub-basins (Section 4.2.3).

4.2.1 Central Outer Cilicia Basin main thrust

The Central OCB main thrust (Fig. 8) is a top-to-the-north deep-rooted thrust fault system that bounds the northern and southern OCB sub-basins, leading to prominent syntectonic wedges (Figs. 7, Suppl. B & C). Around 20 km farther east than the Case Line, the seismic reflection image with higher resolution (from the 2008 seismic campaign) (Fig. 8) illustrates the main thrust tip and the change in seafloor bathymetry at ~1 km water depth. Westwards, the Central OCB main thrust changes from a single fault (Fig. 8) to several thrusts (Fig. 9-E). Thrusts offset both the M- (up to ~100 m) and the N- reflectors, and are only partially influenced by diapirism, as shown by several ramp anticlines

underneath (Figs. 7 & 9-E). The tips of these E-W trending thrusts are evidenced by reverse offsets, northward step-down of unit boundaries, and Unit 1 reflections, as well as the sea floor bulges (Fig. 9-E). The frontal and second sliver thrust tips are expressed as bulges in the seafloor in all three lines, within a concave area ~5–10 km long, while bulges located southward attenuate and eventually dim toward the east (Fig. 7, Suppl. B & C).

Figure 8. The Central OCB main thrust, as shown in a crop of a seismic reflection image to the east of the Case Line. The image shows the depth difference between northern and southern sectors of the OCB and the steepness of the thrust faults, in TWT. Source: Piri Reis Seismic Reflection Profiles (2008 campaign).

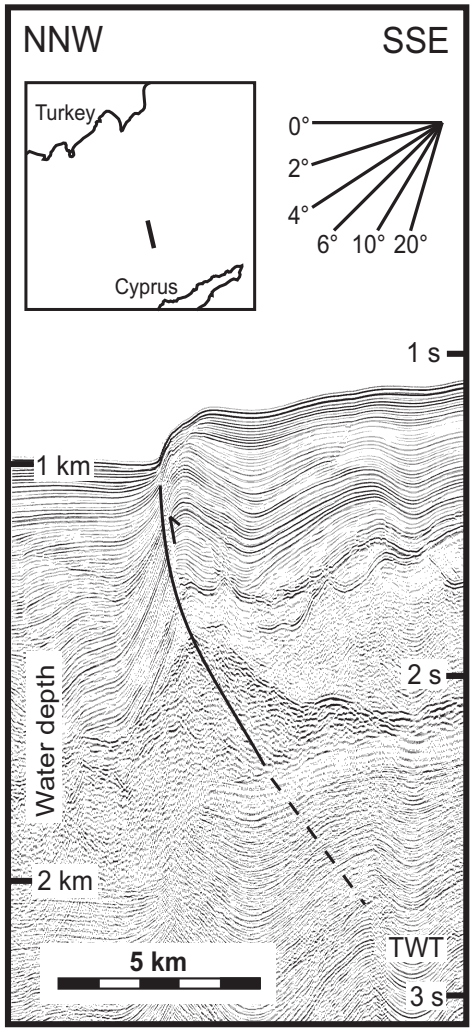

4.2.2 Northern Outer Cilicia Sub-Basin

The sea floor of the northern OCB sub-basin dips south very gently and deepens in a continuous manner from the Turkish break-of-slope. Unit 1 (latest Messinian - Recent) contains two fault systems in the north of the OCB (Figs. 7 & 10). The youngest is an extensional fault system dipping south that reaches the sea floor of the shelf break-of-slope and soles into a single structure parallel to the reflections (Fig. 7). The oldest is a series of roughly vertical faults with small offset that lie within Unit 3 (pre-Messinian Miocene) and cut the corrugated erosional surface at the base of Unit 1 (Fig. 9-B). The kinematic character of the latter faults is ambiguous as they are steep and their associated reflection offsets are unclear. These faults may represent the local equivalent of the Kozan Fault Zone (Bridge *et al.*, 2005; Burton-Ferguson *et al.*, 2005; Aksu *et al.*, 2014), which is mapped farther northeast as a wide transtensional fault system with sinistral offset. The total down-to-basin offset of the top of Unit 3 across the fault system is ~150 m (Figs. 7 & 9-B). Regardless of their kinematics and significance, these faults occur in an inflexion area of the Unit 3 upper boundary, which transitions basinward from gently to distinctly south dipping (Fig. 9-A to C). Unit 1 (latest Messinian - Recent) reflections have a similar change in geometry, dipping gently south. Reflections onlap at low-angle the erosional surface north of the faults (Fig. 9-A), and lie in dip-slopes and at higher angles basinwards (Fig. 9-C).

Figure 9. Depth-converted Case Line is shown at the centre, and used to locate the main features observed along the OCB, which are shown in the different insets. Each inset shows the seismic image in time, the seismic image with traced reflections, and the schematic representation of the observed structures and sedimentary geometries seen along the seismic lines. In the traced image, reflections within the units are shown in red and the reflections in green define boundaries between units.

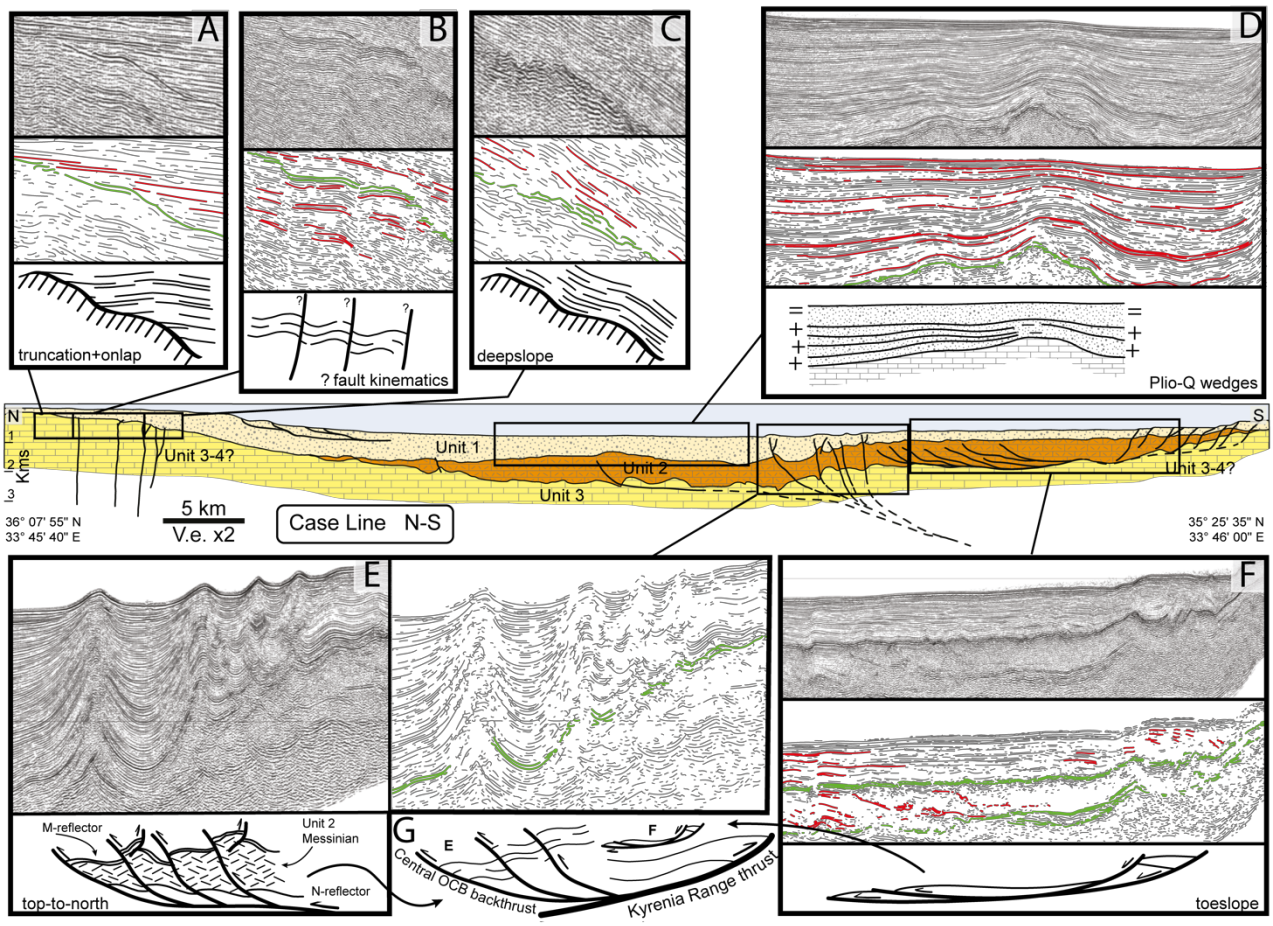

4.2.3 Southern Outer Cilicia Sub-Basin

The sea floor of the southern OCB sub-basin dips north with variable slopes, and shows a corrugated nature and a step-like bathymetry farther south. Two fault systems, one extensional and one contractional, root at the base of Unit 2 (Messinian) (Figs. 7 & 9). At proximal positions, the extensional fault system transects the boundaries of Unit 1 and Unit 2 with increasing offsets southward (Fig. 7). These normal faults displace the sea floor by >80 m leading to a step-like bathymetry that alternates gentle south-dipping with steep north-dipping slopes, while deepening ~300 m northward in ~10–15 km. Total offset increases eastward (cf. Figs. 7, Suppl. B & C). Many of these normal faults vary from subvertical at the sea floor to low angle at depth and probably sole into a sub-horizontal surface. At distal positions, an imbricated system of top-to-the-north low-angle faults sole

out into the base of the Messinian unit (Figs 8 & 10-F). These thrusts, collectively named reflector package "α" in Aksu et al. (2005a), offset several reflections within Unit 2 and form a gentle syncline-anticline succession in Unit 1 without cutting the Unit 2 upper boundary (Fig. 7). Here, the relatively flat sea floor gently increases from 800 m to 900 m in depth over 15–20 km northwards.

5. Onshore-offshore linkage across the plateau margin

We recognise three structures of regional relevance: a monocline in the north, a deep-rooted thrust system in the centre, and a toe-slope system in the south. The latter two structures are controlled by the south-verging thrusts of the Kyrenia Range (Fig. 9-G). The first of these, the Central OCB main thrust (Figs. 8 & 9-E) functions as a back-thrust linked to the Kyrenian culmination, and perches on the southern half of the OCB (Suppl. D). The second, the toe-slope system (Fig. 9-F), is a gravitational kinematic response to the slope instabilities in the margin of the perched basin, aid by the mobility of the Messinian layer (Suppl. E). Below, we focus exclusively on the deformation and sedimentary patterns resulting from the growth of the third structure —the Miocene monocline of south Turkey. We reconstruct the monocline by coupling onshore and offshore geology across the southern margin of the Central Anatolian Plateau (SCAP) (Fig. 11). We consider the kink structure on the Turkish shelf (Fig. 9-A,-B,-C) as kinematically linked with the equivalent, albeit larger, monocline flexure observed in the Mut Basin (Fig. 5), and apply inferences on the kinematics of the former (section below) to the latter.

5.1 Late Miocene to Recent kinematics

On the upper sector of the Turkish shelf, the reflections of Unit 1 (latest Messinian - Recent) onlap the erosional contact with Unit 3 (pre-Messinian Miocene) (Fig. 9-A). Unit 1 reflectors progressively pass basinward to dip-slope geometries (Fig. 9-C), developing syntectonic wedges that open in the same direction (Fig. 11). The scale of these wedges dictate that they are not the result of climatic oscillations. We distinguish different sub-units within Unit 1 and analyse the location of the transition between onlap and dip-slope reflectors. Younger sub-units have the onlap-dip slope transition at northward locations and develop syntectonic unconformities and on-structure wedges, i.e. cover both limbs of the fold (see Patton, 2004 for terminology) (subunits 1–4; Fig. 11). This geometrical pattern suggests that a continuous increase in accommodation space alternates with abrupt decreases during fold-kink growth (Riba, 1976; Patton, 2004). Although sedimentation entering the system laterally could produce similar patterns, parallel horizontal reflections in the upper part the sequence suggests subsidence (or sea level rise). Located at the top of the seismo-stratigraphic sequence, sub-unit 5 is the first sub-unit that is not wedged, which indicates self-similar growth of the structure until close to recent times (Fig. 10). Sub-unit 6 formed as a block at younger times.

The underlying reflections of Unit 3 (pre-Messinian Miocene) are cut by the erosional surface. Roughly vertical faults transect Unit 3 reflections in the axial plane of a kink structure (Fig. 9-B); whereas Unit 3 reflections are subhorizontal in the northern areas and disrupted where faults offset the unit, they dip 25–30° basinward to the south (Figs. 9-A,-C and 10). These geometrical relationships indicate that the kink monocline developed after deposition of at least part of Unit 3 (pre-Messinian Miocene), but prior to the onset of erosion.

Figure 10. A) Seismic image in time with traced reflections showing the angular relationships and main geometries seen in the Plio-Q and Miocene units in the South Turkish offshore. Distinct onlap-wedging characteristics allow for the differentiation of six sequential packages, numbered from oldest to youngest. Representative dips of reflections of both units are shown in blue. B) Conceptual evolution of the south margin of the CAP, as derived from the analysis of seismic reflections in the northern boundary of the OCB.

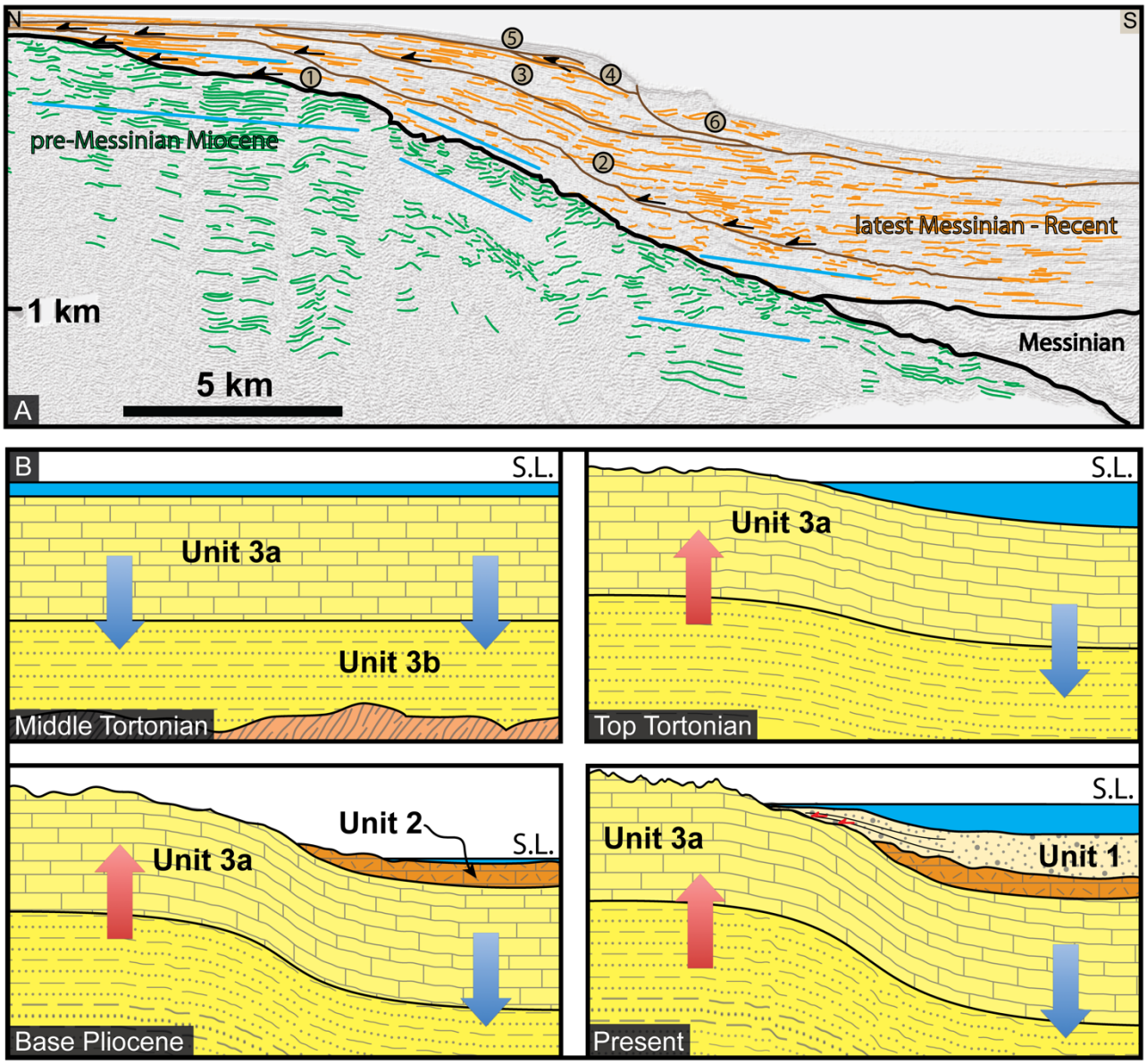

5.2 Geologic onshore-offshore cross-sections

We reconstruct two onshore-offshore cross-sections linking geological observations across the SCAP margin. We attempt to overcome the lack of data coverage and/or the discontinuity of Miocene rocks near the Turkish coast, using a different approach to reconstruct each of the two onshore-offshore cross-section. The transect on the SE plateau margin (Fig. 11-A) has the largest data coverage, i.e. the offshore seismic line reaches the closest to the coast in which Miocene rocks outcrop. However, the northward continuation of the offshore line towards the onshore meets basement rocks, and both sections are a considerable distance apart. The transect on the S plateau margin (Fig. 11-B) has the tightest age constraints, i.e. accurate dating of the youngest pre-Messinian Miocene rocks onland and a good age estimate of its corresponding offshore unit (see Fig. 2). However, age error bars and uncertainties are still large, and both correlatable units are a substantial distance apart. We use the transects with caution to provide first-order estimations of geometry, vertical displacement and shortening across the monocline.

The onshore-offshore transect on the SE plateau margin (Fig. 11-A) uses Section B in the Mut Basin (Fig. 6-B) as the continuation of the depth-converted Case Line (Fig. 7, bottom). We use bed dips from the field and reflectors from the depth-converted Case Line (Fig. 10-A). Figure 12-A depicts in red a "key bed" to characterise the first-order geometry of the regional Miocene monocline structure on its flank. This "key bed" represents a rock layer that is (i) at the lowest possible elevation above topography onshore, as a proxy to a rock layer that is slightly younger than the mid-Miocene outcropping rocks; and (ii) at the highest possible elevation below the erosional surface offshore, as a proxy to a rock layer that is slightly older than Messinian. We thus consider the "key bed" loosely as Tortonian. We obtain the "key bed" in the onshore profile by

extrapolating vertically up the bed attitude data of the first Middle Miocene appearance atop basement, and in the offshore by extrapolating vertically down reflections northwards from the contact between the erosional surface and the Messinian unit. Given that the Tortonian could be at higher elevations onland and at deeper levels offshore, the steepness of the flank is a minimum estimate, and thus the monocline may accommodate larger relative vertical displacement than that shown in Fig. 11-A.

Figure 11. Onshore-offshore geologic cross-section in S Turkey. The red line represents a key layer that represents approximately a bed of Tortonian age, and relates with the minimum possible relative vertical displacement within the Miocene rocks that shape the monocline. A. Onshore and offshore geometries of the Miocene deposits and their relationships with the basement. B. Onshore and offshore link of rocks of Late Miocene age. (a) is based on Cosentino et al. (2012), (b) is obtained from the MTA geologic maps of Adana 1:500.000 (Ulü, 2002), and (c) and (d) are from Seismic Line Suppl. C.

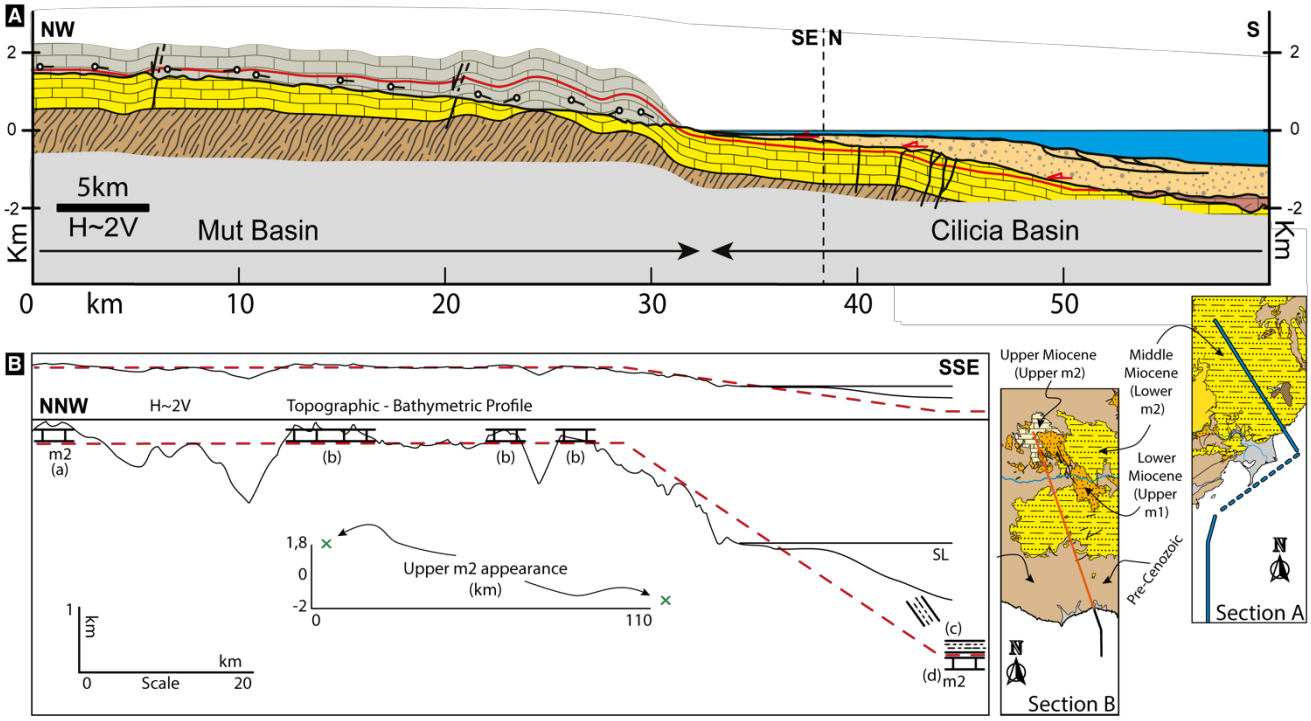

The onshore-offshore transect on the S plateau margin (Fig. 11-B) has the age constraints of Cosentino et al. (2012) onshore, and Aksu et al. (2005a) offshore. The shallow water limestones exposed onshore at the upper section of Unit "m2" in the Geological Map of the Adana Plate [1:500,000] (Ulu, 2002) are Late Tortonian, ~8 Ma (Cosentino *et al.*, 2012) (a, in Fig. 11-B). The offshore Unit 3a, seen as fluvio-deltaics in the exploration wells correlates with onshore formations of age base Tortonian, ~11 Ma (Aksu *et al.*, 2005a) (d in Fig. 11-B; Fig. Suppl. C). Here, the "key bed" that helps constrain to a first order the geometry of the monocline runs below the Upper Tortonian onland (a in Fig. 11-B) and above the Lower Tortonian offshore (d in Fig. 11-B), and is thus, again, loosely Tortonian in age. The "key bed" transects in a horizontal line Tortonian or older rocks on land (b in Fig 11-B) and either Tortonian or younger rocks offshore (c in Fig. 11-B represents the base of the latest Messinian). Therefore, geometrical constraints for the "key bed" result only from restrictions by the topography near the Turkish coast that is devoid of Miocene rocks. Linking both "m2" appearances onshore and offshore imposes a minimum boundary for the steepness of the monocline flank (Fig. 11-B).

We characterise a minimum-amplitude monocline geometry and infer steep Miocene beds for the monocline flank, linking onland and offland sectors with gentle south dips (Fig. 11). Geometrical constraints set by the "key bed" suggest that the monocline flank has a maximum horizontal length of 20–25 km. Similarly, the "key bed" in both figures provides an estimate of the minimum vertical relative displacement cross the SCAP margin. Rocks depositing close to sea level show surface uplift of 1.8 km (a in Fig. 11-B) mirrored by ~2 km of absolute subsidence (d in Fig. 11-B) during monocline growth. Therefore, the relative vertical displacement since the Tortonian is ~3.8 km, which provides a rough average rate of vertical displacement of ~0.5 mm/y. The "key bed" allows shortening estimates of <1 % across the fold structure (in 110 km for the

section in Fig. 11-B). In our approximations to the monocline geometry, axial planes of the monocline kinks are almost parallel and seem to converge only at significant depths.

6. Discussion: Monoclinal growth of the plateau margin in S Turkey

Our onshore-offshore approach allows insights on the accommodation and growth mechanics of the SCAP, provides constraints on its time and mode of (de)formation, and sets the plateau margin in the regional context of the Cyprus subduction to the south.

6.1. Time of vertical motions

Our data suggest that vertical tectonic motions in the SCAP started >5 Ma and that relevant relief in the modern Central Taurides existed at ~5 Ma. Late Miocene shallow marine rocks shaping the monocline outcrop in its uplifting sectors, and feed the thick depocentres of latest Messinian to Present sediments in its subsiding sectors (Figs. 5, 7 & 11). The lateral continuity of dip-sloping Miocene rocks throughout the Mut Basin (Fig. 5) implies that most of the Miocene succession deposited prior to monocline growth. Later uplift exposed the Late Miocene rocks, truncating and eroding the series (Fig. 10) while subsiding sectors of the monocline continued deposition throughout the latest Messinian - Recent times (Fig. 7, 10, Suppl. B & Suppl. C). Removal of substantial amounts of sediments from the rising Central Taurides since the latest Messinian (Walsh-Kennedy *et al.*, 2014) led to a continuous stack of prominent delta lobes in the Göksu Delta (Aksu *et al.*, 2014), and the syntectonic wedges on top of Late Miocene erosional surface (Fig. 10). The above evidence is at odds with fast growth of topography after the Early Pleistocene (Schildgen *et al.*, 2012) or the early Middle Pleistocene (Öğretmen *et al.*,

2018). Contrarily, the continued growth since latest Miocene of the Göksu Delta and near-coast syntectonic wedges, as well as the overall low gradient stream and a wide valley floor (often >30 km in width) of the Göksu River (Figs. 4 and 5), are consistent with the presence of relevant (km-scale) topography in the Central Taurides before the Pliocene (Fernández-Blanco, 2014; Meijers *et al.*, 2018).

6.2. Accommodating structures

The flexural monocline in S Turkey is the only structure capable of accommodating the ~4 km vertical gradient in Miocene rocks observed at present across the SCAP (Fig. 11). The growth of the regional flexural monocline accommodates most, if not all, the counter-acting vertical motions. Concomitant vertical motions of short wavelength led the surface uplift of S Turkey that emerged and disconnected the Mut Basin, as well as the counter-balancing subsidence of the Cilicia Basin. The present-day geometry of the monocline implies a narrow area of deformation (~20-25 km) and suggest southward strain propagation in a kink-band fashion. The fact that the axial planes of the kink-band are almost parallel between them precludes calculus of the depth of the tip of the potential fault responsible for the kink-band, and suggest that, if any such fault exists, it is likely to be located below the upper crustal depths. Strain accumulation at depth is at variance with a potential accommodating structure close underneath the succession, regardless of its kinematics.

Other known structures cannot accommodate the motions. Late Miocene and younger minor normal and strike-slip faulting exists in the modern Central Taurides (Ilgar & Nemec, 2005) and significant extensional and/or strike-slip faults occur to its sides (Aksu *et al.*, 2005a, 2014). The most prominent of these fault systems, the Kozan Fault Zone

(KFZ), at the south-eastern margin of the modern Central Taurides, has vertical offsets of ~50-200 ms in the M-reflector, and sinistral displacements of ~20-35 km in the uppermost Messinian to Quaternary deposits of the Göksu Delta (Aksu *et al.*, 2014). The amplitude of the monocline is, ad minimum, one order of magnitude larger than vertical displacements along the KFZ (Aksu *et al.*, 2014). Moreover, transtension along the KFZ ensued during the onset of the westward motion of Aegean-Anatolia plate (Aksu *et al.*, 2014), and thus postdates the majority of the uplift. Therefore, the KFZ potential contribution to monoclinal growth is trivial and associated strain is not related to the main geodynamic causes behind the motions discussed in this contribution. We suggest that the mechanical load of Taurides aids subsidence of its external areas, and speculate that this isostatic gradient guides the entrenchment of the KFZ between both regions.

6.3. Tectonic regime and contextualization

Shortening in Miocene and younger rocks record compression in south Turkey, in the offshore and along the Central Cyprus margin during growth of the southern margin of the Central Anatolian Plateau (Figs. 6 to 11). In the Mut Basin, shortening is observed at several scales; Miocene infill rocks striking parallel and dipping orthogonal to basement ridges outcropping parallel to the coast (Fig. 5); asymmetric Miocene folds having steeper southern flanks, and; reverse faulting during deposition of Middle Miocene rocks (Fig. 6). Shortening in the Turkish shelf results in latest Miocene-Recent on-structure syntectonic wedges that open southward (Fig. 10). Farther south, all other coeval regional-scale structures along the Central Cyprus margin developed by shortening (Figs. 7, 8, 9 and Suppl. B to E). Although monoclines grow by many different structural mechanisms (e.g., Freund, 1979; Reches *et al.*, 1981; Tindall & Davis, 1999; Willsey *et al.*, 2002; Patton,

2004), the structures described above report compressional stresses before, during and after the time of formation of the flexural monocline, and thus strongly suggest monocline growth by shortening.

Convergence between Africa/Arabia and Eurasia results in overall N-S compression between S Turkey and the Cyprus trench. Subduction results in Miocene contraction and Plio-Quaternary strain partitioning, by which coeval thrust tectonics and left-lateral oblique stretching occur in east- and northeast-trending sectors, respectively, of the south-arched, crustal-scale thrust systems of Misis-Kyrenia Fault Zone, Amanos-Larnaka Fault Zone and the Cyprus Arc itself (e.g., Aksu *et al.*, 2005a, 2005b, 2014; Burton-Ferguson *et al.*, 2005; Calon *et al.*, 2005a, 2005b; Hall *et al.*, 2005a, 2005b; Işler *et al.*, 2005). Shortening tectonics in the Outer Cilicia Basin resulted in contractional structures during the Late Miocene and the mid-Pliocene or younger times (Suppl. Mat. D & E), while transtension is clear in the southeastern sectors of the Turkish shelf and eastwards (Aksu *et al.*, 2014). Our field evidence for the Central Taurides suggest that (i) the monocline has a south-arched geometry that follows roughly the coast; (ii) shortening might have initiated as early as Middle Miocene (Fig. 6) and; (iii) joint deformation of pre-Miocene basement and Late Miocene rocks occurred during post-Miocene times (Fig. 5; section 3.2). For similar and younger time frames, other studies report normal and strike-slip faults (Ilgar & Nemec, 2005). Taken together, we infer that the evolution of S Turkey is comparable to that of arc-parallel regional structures farther south. Similar to these regional-scale structures, albeit devoid of regional ground-breaking faults, in the Central Taurides, subduction-related shortening coexists with, and may be partially overprinted by, extrusion-related transtensional structures since latest Messinian.

Shortening and uplift in the SCAP led by protracted contraction along the Central Cyprus continental margin contextualize the plateau margin as the forearc high of the

Central Cyprus forearc basin system (Fig. 12). Although the Central Cyprus continental margin has varied in space and time, shortening leading to the growth of structural highs and associated south-tapering forearc basins south of Turkey has been occurring since the slab retreated to close to its present position at ~25 My (Robertson, 1998). The trench lies at present south of Cyprus, between the Eratosthenes Seamount and the Troodos ophiolite (Robertson, 1998). Northwards, thrusting along the Kyrenian culmination formed the Kyrenia Range, and its southwards emplacement led to the Messaoria Basin (Calon *et al.*, 2005a, 2005b; McCay, 2010). They are the trench-slope break and a wedge-top basin. Further north along the margin, the OCB and the Mut Basin are the residual and intramassif forearc basins fragmented by the Central Taurides forearc high (Fig. 12). Mio-Pliocene north-verging thrusts north of the Central Taurides (Gürer, 2017) may function as antithetic structures to the monocline, suggesting forearc high uplift as a wide anticlinorium during contraction and crustal thickening below the modern Central Taurides. Farther north, the volcanic arc of Cappadocia has calc-alkaline magmas with clear subduction signals since ~13 Ma (e.g., Aydar, 1998) with younger magmas at southwestward locations increasing in within-plate character since ~6-7 Ma (e.g., Deniel *et al.*, 1998). Although the latter has been linked to asthenospheric sources (e.g., Göğüş *et al.*, 2017), heterogeneous lithospheric sources are deduced from Quaternary calc-alkaline/alkaline penecontemporaneous magmas suites (Dogan-Kulahci *et al.*, 2018).

Figure 12. Transect across the Central Cyprus accretionary wedge (at ~33°30' E). The transect shows the correlation between the main tectonostraigraphic features of the Central Cyprus margin and elements of a "standard" accretionary margin with forearc high. Slightly modified from Fernández-Blanco, 2014.

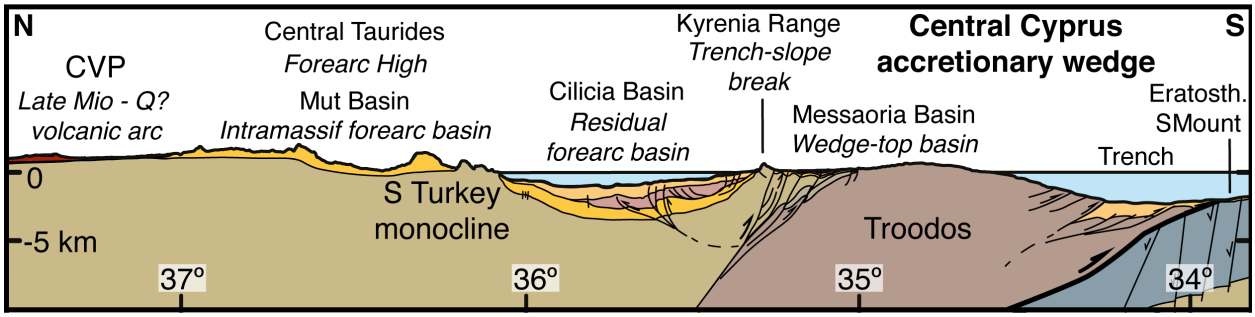

6.4. Mode of plateau margin growth

Monoclinal flexure during growth of the plateau margin before the Pliocene agrees well with paleoaltimetry estimations of ~2 km of relief at ~5 Ma (Meijers *et al.*, 2018) and the subsidence signal thereafter (Walsh-Kennedy *et al.*, 2014). Contraction at depth, crustal thickening and monocline growth are also compatible with the presence of the Central Cyprus slab, and the thick crust below the modern Central Taurides relative to the Central Anatolia Plateau interior (e.g., Bakırcı *et al.*, 2012; Abgarmi *et al.*, 2017; Delph *et al.*, 2017; Portner *et al.*, 2018). By contrast, alternative models proposing plateau margin uplift by shallow slab break-off during a multi-phase evolution (Cosentino *et al.*, 2012; Schildgen *et al.*, 2012, 2014; Öğretmen *et al.*, 2018) are inconsistent with the aforementioned research. In brief, evidence shown here puts into question "passive" isostatic uplift models for the southern margin of the Central Anatolian Plateau and points instead to "active" contractional margin growth.

We suggest plateau margin growth by plate thickening and strain accumulation at depth, as led by thermal weakening and viscous flow in the lower crust (Fuller *et al.*, 2006; Fernández-Blanco *et al.*, 2012). Thermally-activated viscous flow and ductile strain at deeper sectors of orogenic subduction wedges may explain advanced stages of evolution in forearcs and the development of forearc highs (Pavlis & Bruhn, 1983; Pope & Willett, 1998; Fuller *et al.*, 2006; Willett & Schlunegger, 2010). Applied to the southern margin of

the Central Anatolian Plateau, this mechanism would imply that protracted thickening by sedimentary accretion from the Central Cyprus margin thermally activates low-strength viscous flow at the base of the Anatolian crust, and sustains the growth of the SCAP as a regional flexure at plateau margin scale.

7. Conclusion

Geological evidence across the southern margin of the Central Anatolian Plateau and farther south suggests that the plateau margin developed prior to the Pliocene by shortening led by Eurasia-Africa compression. Accounting for the location, attitude and timing of first-order structures in the onshore, as well as the kinematics, tectonic regime and age of regional accommodating structures in the offshore, we infer a flexural monocline in Miocene rocks at the scale of the plateau margin. Monocline growth during post-Miocene times can explain surface uplift in the Mut Basin and its regional coupling with concomitant, short wavelength subsidence in the Cilicia Basin. We characterize the monocline as a regional kink-band fold where two gently south-dipping domains are separated by a narrow flank of ~20-25 km. The Miocene rocks have relative vertical displacement rates of ~0.5 mm/y and shortening < 1% (in 110 km). Miocene monocline wavelength and geometry are indicative of plateau margin growth in relation to deep-sourced deformation, that we understand in the context of upper crustal flexure during the development of the forearc high of the Cyprus subduction system.

Acknowledgements

The authors would like to thank the masterful editorial management of Atle Rotevatn, and the reviews by Gilles Brocard, Enrico Tavarnelli and two anonymous colleagues. We thank the Netherlands Organisation for Scientific Research (NWO) for funding this study, part of the Vertical Anatolian Movement Project (VAMP), an ESF EuroCORE TOPOEurope. DFB is deeply thankful to Fabrizio Pepe, who provided and helped with the GeoSuite AllWorks software. Contributions from AA and JH are supported by research grants from the Natural Sciences and Engineering Research Council of Canada. Authors have no conflict of interest to declare.

References

ABGARMI, B., DELPH, J.R., ARDA OZACAR, A., BECK, S.L., ZANDT, G., SANDVOL, E., TURKELLI, N., AND BERK BIRYOL, C. (2017) Structure of the crust and African slab beneath the central Anatolian plateau from receiver functions: New insights on isostatic compensation and slab dynamics. *Geosphere* 13, 1774–1787.

AKSU, A.E., CALON, T.J., HALL, J., MANSFIELD, S. & YAŞAR, D. (2005A) The Cilicia–Adana basin complex, Eastern Mediterranean: Neogene evolution of an active fore-arc basin in an obliquely convergent margin. *Marine Geology* 221, 121–159.

AKSU, A.E., CALON, T.J., HALL, J. & YAŞAR, D. (2005B) Origin and evolution of the Neogene Iskenderun Basin, northeastern Mediterranean Sea. *Marine Geology* 221, 161–187.

AKSU, A.E., WALSH-KENNEDY, S., HALL, J., HISCOTT, R.N., YALTIRAK, C., AKHUN, S.D. & ÇIFÇI, G. (2014) The Pliocene–Quaternary tectonic evolution of the Cilicia and Adana basins, eastern Mediterranean: Special reference to the development of the Kozan Fault zone. *Tectonophysics* 622, 22–43.

ALLMENDINGER, R., JORDAN, T., KAY, S. & ISACKS, B. (1997) The evolution of the Altiplano-Puna plateau of the Central Andes. *Annual review of earth and planetary sciences* 25, 139–174.

AYDAR , E. (1998) Early Miocene to Quaternary evolution of volcanism and the basin formation in western Anatolia: a review. *Journal of Volcanology and Geothermal Research* 85, 69–82.

ANDREW, T. & ROBERTSON, A.H.F. (2002) The Beyşehir–Hoyran–Hadim Nappes: Genesis and emplacement of Mesozoic marginal and oceanic units of the northern Neotethys in southern Turkey. *Journal of the Geological Society* 159, 529–543.

BAKIRCI, T., YOSHIZAWA, K. & ÖZER, M. (2012) Three-dimensional S-wave structure of the upper mantle beneath Turkey from surface wave tomography. *Geophysical Journal International* 190, 1058–1076.

BALLATO, P., MULCH, A., LANDGRAF, A., STRECKER, M.R., DALCONI, M.C., FRIEDRICH, A. & TABATABAEI, S.H. (2010) Middle to late Miocene Middle Eastern climate from stable oxygen and carbon isotope data, southern Alborz mountains, N Iran. *Earth and planetary science letters* 300, 125–138.

BARTOL, J. & GOVERS, R. (2014) A single cause for uplift of the Central and Eastern Anatolian plateau? *Tectonophysics* 637, 116–136.

BASSANT, P., VAN BUCHEM, F.S.P., STRASSER, A. & GÖRÜR, N. (2005) The stratigraphic architecture and evolution of the Burdigalian carbonate—siliciclastic sedimentary systems of the Mut Basin, Turkey. *Sedimentary Geology* 173, 187–232.

BIRD, P. (1979) Continental delamination and the Colorado Plateau. *Journal of Geophysical Research, [Solid Earth]* 84, 7561–7571.

BIRYOL, C., BECK, S.L., ZANDT, G. & ÖZACAR, A. (2011) Segmented African lithosphere beneath the Anatolian region inferred from teleseismic P-wave tomography. *Geophysical Journal* 184, 1037–1057.

BRIDGE, C., CALON, T.J., HALL, J. & AKSU, A.E. (2005) Salt tectonics in two convergent-margin basins of the Cyprus arc, Northeastern Mediterranean. *Marine Geology* 221, 223–259.

BURTON-FERGUSON, R., AKSU, A.E., CALON, T.J. & HALL, J. (2005) Seismic stratigraphy and structural evolution of the Adana Basin, eastern Mediterranean. *Marine Geology* 221, 189–222.

CALON, T.J., AKSU, A.E. & HALL, J. (2005A) The Neogene evolution of the Outer Latakia Basin and its extension into the Eastern Mesaoria Basin (Cyprus), Eastern Mediterranean. *Marine Geology* 221, 61–94.

CALON, T.J., AKSU, A.E. & HALL, J. (2005B) The Oligocene-Recent evolution of the Mesaoria Basin (Cyprus) and its western marine extension, Eastern Mediterranean. *Marine Geology* 221, 95–120.

CIPOLLARI, P., HALÁSOVÁ, E., GÜRBÜZ, K. & COSENTINO, D. (2013) Middle-Upper Miocene paleogeography of southern Turkey: insights from stratigraphy and calcareous nannofossil biochronology of the Olukpınar and Başyayla sections (Mut-Ermenek Basin). *Turkish Journal of Earth Sciences* 22, 820–838.

ÇINER, A., KARABIYIKOĞLU, M., MONOD, O., DEYNOUX, M. & TUZCU, S. (2008) Late Cenozoic Sedimentary Evolution of the Antalya Basin, Southern Turkey. *Turkish Journal of Earth Sciences* 17, 1–41.

CLARK, M.K. (2012) Continental collision slowing due to viscous mantle lithosphere rather than topography. *Nature* 483, 74–77.

CLARK, M. & ROBERTSON, A. (2002) The role of the Early Tertiary Ulukisla Basin, southern Turkey, in suturing of the Mesozoic Tethys ocean. *Journal of the Geological Society* 159, 673–690.

CLARK, M. & ROBERTSON, A. (2005) Uppermost Cretaceous–Lower Tertiary Ulukışla Basin, south-central Turkey: sedimentary evolution of part of a unified basin complex within an evolving Neotethyan suture zone. *Sedimentary Geology* 173, 15–51.

COSENTINO, D., BUCHWALDT, R., SAMPALMIERI, G., IADANZA, A., CIPOLLARI, P., SCHILDGEN, T.F., HINNOV, L.A., RAMEZANI, J. & BOWRING, S.A. (2013) Refining the Mediterranean "Messinian gap" with high-precision U-Pb zircon geochronology, central and northern Italy. *Geology* 41, 323–326.

COSENTINO, D., SCHILDGEN, T., CIPOLLARI, P., FARANDA, C., GLIOZZI, E., HUDÁČKOVÁ, N., LUCIFORA, S. & STRECKER, M.R. (2012) Late Miocene surface uplift of the southern margin of the Central Anatolian Plateau, Central Taurides, Turkey. *GSA Bulletin* 124, 133–145.

DELPH, J.R., ABGARMI, B., WARD, K.M., BECK, S.L., ARDA ÖZACAR, A., ZANDT, G., SANDVOL, E., TÜRKELLI, N., AND KALAFAT, D. (2017) The effects of subduction termination on the continental lithosphere: Linking volcanism, deformation, surface uplift, and slab tearing in central Anatolia. *Geosphere* 13, 1788–1805.

DENIEL, C., AYDAR, E. & GOURGAUD, A. (1998) The Hasan Dagi stratovolcano (Central Anatolia, Turkey): evolution from calc-alkaline to alkaline magmatism in a collision zone. *Journal of Volcanology and Geothermal Research* 87, 275–302.

DOGAN-KULAHCI, G.D., TEMEL, A., GOURGAUD, A., VAROL, E., GUILLOU, H. & DENIEL, C. (2018) Contemporaneous alkaline and calc-alkaline series in Central Anatolia (Turkey): Spatio-temporal evolution of a post-collisional Quaternary basaltic volcanism. *Journal of Volcanology and Geothermal Research* 356, 56–74.

ERIŞ, K.K., BASSANT, P. & ÜLGEN, U.B. (2005) Tectono-stratigraphic evolution of an Early Miocene incised valley-fill (Derinçay Formation) in the Mut Basin, Southern Turkey. *Sedimentary Geology* 173, 151–185.

EVANS, G., MORGAN, P., EVANS, W.E., EVANS, T.R. & WOODSIDE, J.M. (1978) Faulting and halokinetics in the northeastern Mediterranean between Cyprus and Turkey. *Geology* 6, 392–396.

FARANDA, C., GLIOZZI, E., CIPOLLARI, P., GROSSI, F., DARBAŞ, G., GÜRBÜZ, K., NAZIK, A., GENNARI, R. & COSENTINO, D. (2013) Messinian paleoenvironmental changes in the easternmost Mediterranean Basin: Adana Basin, southern Turkey. *Turkish Journal of Earth Sciences* 22, 839–863.

FERNÁNDEZ-BLANCO, D. (2014) Evolution of Orogenic Plateaus at Subduction Zones: Sinking and raising the southern margin of the Central Anatolian Plateau. Amsterdam: Vrije Universiteit.

FERNÁNDEZ-BLANCO, D. & BERTOTTI, G. (2012) Neogene vertical tectonics of the south margin of the Central Anatolia plateau in relation to Cyprus Arc subduction. *AGU Fall Meeting*.

FERNÁNDEZ-BLANCO, D., GIOVANNI, B. & ATTILA, Ç. (2013) Cenozoic tectonics of the Tuz Gölü Basin (Central Anatolia Plateau, Turkey). *Turkish Journal of Earth Sciences* 22, 715–738.

FREUND, R. (1979) Progressive strain in beds of monoclinal flexures. *Geology* 7, 269–271.

FULLER, C.W., WILLETT, S.D. & BRANDON, M.T. (2006) Formation of forearc basins and their influence on subduction zone earthquakes. *Geology* 34, 65–68.

GARCIA-CASTELLANOS, D. (2007) The role of climate during high plateau formation. Insights from numerical experiments. *Earth and planetary science letters* 257, 372–390.

GÖĞÜŞ, O.H. & PYSKLYWEC, R.N. (2008) Mantle lithosphere delamination driving plateau uplift and synconvergent extension in eastern Anatolia. *Geology* 36, 723–726.

GÖĞÜŞ, O.H., PYSKLYWEC, R.N., ŞENGÖR, A.M.C. & GÜN, E. (2017) Drip tectonics and the enigmatic uplift of the Central Anatolian Plateau. *Nature communications* 8, 1538.

GORUR, N., OKTAY, F.Y., SEYMEN, I. & SENGÖR, A.M.C. (1984) Palaeotectonic evolution of the Tuzgolu basin complex, Central Turkey: sedimentary record of a Neo-Tethyan closure. *Geological Society of London Special Publications* 17, 467–482.

GÜRER, M.D. (2017) Subduction evolution in the Anatolian region: the rise, demise, and fate of the Anadolu Plate. University Utrecht

HALL, J., AKSU, A.E., CALON, T.J. & YAŞAR, D. (2005A) Varying tectonic control on basin development at an active microplate margin: Latakia Basin, Eastern Mediterranean. *Marine Geology* 221, 15–60.

HALL, J., CALON, T.J., AKSU, A.E. & MEADE, S.R. (2005B) Structural evolution of the Latakia Ridge and Cyprus Basin at the front of the Cyprus Arc, Eastern Mediterranean Sea. *Marine Geology* 221, 261–297.

HSÜ, K.J., RYAN, W.B.F. & CITA, M.B. (1973) Late Miocene desiccation of the Mediterranean. *Nature* 242, 240–244.

HUVAZ, O. (2009) Comparative petroleum systems analysis of the interior basins of Turkey: Implications for petroleum potential. *Marine and Petroleum Geology* 26, 1656–1676.

ILGAR, A. & NEMEC, W. (2005) Early Miocene lacustrine deposits and sequence stratigraphy of the Ermenek Basin, Central Taurides, Turkey. *Sedimentary Geology* 173, 233–275.

IMPRESCIA, P., PONDRELLI, S., VANNUCCI, G. & GRESTA, S. (2012) Regional centroid moment tensor solutions in Cyprus from 1977 to the present and seismotectonic implications. *Journal of Seismology* 16, 147–167.

IŞLER, F.I., AKSU, A.E., HALL, J., CALON, T.J. & YAŞAR, D. (2005) Neogene development of the Antalya Basin, Eastern Mediterranean: An active forearc basin adjacent to an arc junction. *Marine Geology* 221, 299–330.

JANSON, X., VAN BUCHEM, F.S.P., DROMART, G., EICHENSEER, H.T., DELLAMONICA, X., BOICHARD, R., BONNAFFE, F. & EBERLI, G. (2010) Architecture and facies differentiation within a Middle Miocene carbonate platform, Ermenek, Mut Basin, southern Turkey. *Geological Society, London, Special Publications* 329, 265–290.

KARABIYIKOĞLU, M., ÇINER, A., MONOD, O., DEYNOUX, M., TUZCU, S. & AND ÖRÇEN, S. (2000) Tectonosedimentary evolution of the Miocene Manavgat Basin, western Taurides, Turkey. *Geological Society, London, Special Publications* 137, 271–294.

MCCAY, G. (2010) Tectonic-sedimentary evolution of the Girne (Kyrenia) Range and the Mesarya (Mesaoria) Basin, North Cyprus. PhD. University of Edinburgh

McCAY, G.A., ROBERTSON, A.H.F., KROON, D., RAFFI, I., ELLAM, R.M. & NECDET, M. (2012) Stratigraphy of Cretaceous to Lower Pliocene sediments in the northern part of Cyprus based on comparative 87Sr/86Sr isotopic, nannofossil and planktonic foraminiferal dating. *Geological Magazine* 150, 333–359.

McCAY, G. & ROBERTSON, A. (2012) Late Eocene–Neogene sedimentary geology of the Girne (Kyrenia) Range, northern Cyprus: A case history of sedimentation related to progressive and diachronous continental collision. *Sedimentary Geology* 265, 30–55.

MEIJERS, M.J.M., BROCARD, G.Y., COSCA, M.A., LÜDECKE, T., TEYSSIER, C., WHITNEY, D.L. & MULCH, A. (2018) Rapid late Miocene surface uplift of the Central Anatolian Plateau margin. *Earth and Planetary Science Letters* 497, 29–41.

MONOD, O. (1977) Recherches géologiques dans le Taurus occidental au Sud de Beysehir (Turquie). PhD. Université de Paris-Sud Centre d'Orsay

MONOD, O., KUZUCUOĞLU, C. & OKAY, A.I. (2006) A Miocene palaeovalley network in the Western Taurus (Turkey). *Turkish Journal of Earth Sciences* 15, 1–23.

MULCH, A., GRAHAM, S.A. & CHAMBERLAIN, C.P. (2006) Hydrogen isotopes in Eocene river gravels and paleoelevation of the Sierra Nevada. *Science* 313, 87–89.

NELSON, K.D., ZHAO, W., BROWN, L.D., KUO, J., CHE, J., LIU, X., KLEMPERER, S.L., MAKOVSKY, Y., MEISSNER, R., MECHIE, J., KIND, R., WENZEL, F., NI, J., NABELEK, J., LESHOU, C., TAN, H., WEI, W., JONES, A.G., BOOKER, J., UNSWORTH, M., KIDD, W., HAUCK, M., ALSDORF, D., ROSS, A., COGAN, M., WU, C., SANDVOL, E. & EDWARDS, M. (1996) Partially Molten Middle Crust Beneath Southern Tibet: Synthesis of Project INDEPTH Results. *Science* 274, 1684–1688.

ÖĞRETMEN, N., CIPOLLARI, P., FREZZA, V., FARANDA, C., KARANIKA, K., GLIOZZI, E., RADEFF, G. & COSENTINO, D. (2018) Evidence for 1.5 km of Uplift of the Central Anatolian Plateau's Southern Margin in the Last 450 kyr and Implications for Its Multiphased Uplift History. *Tectonics*, 2017TC004805.

ÖZSAYIN, E., CINER, T.A., ROJAY, F.B., DIRIK, R.K., MELNICK, D., FERNÁNDEZ-BLANCO, D., BERTOTTI, G., SCHILDGEN, T., GARCIN, Y. & MANFRED S AND SUDO (2013) Plio-Quaternary extensional tectonics of the Central Anatolian Plateau: a case study from the Tuz Gölü Basin, Turkey. *Turkish Journal of Earth Sciences* 22, 691–714.

PATTON, T.L. (2004) Numerical models of growth-sediment development above an active monocline. *Basin Research* 16, 25–39.

PAVLIS, T.L. & BRUHN, R.L. (1983) Deep-seated flow as a mechanism for the uplift of broad forearc ridges and its role in the exposure of high P/T metamorphic terranes. *Tectonics* 2, 473–497.

POPE, D.C. & WILLETT, S.D. (1998) Thermal-mechanical model for crustal thickening in the central Andes driven by ablative subduction. *Geology* 26, 511–514.

PORTNER, D.E., DELPH, J.R., BERK BIRYOL, C., BECK, S.L., ZANDT, G., ARDA ÖZACAR, A., SANDVOL, E. & TÜRKELLI, N. (2018) Subduction termination through progressive slab deformation across Eastern Mediterranean subduction zones from updated P-wave tomography beneath Anatolia. *Geosphere* 14, 907–925.

POWELL, C. (1986) Continental underplating model for the rise of the Tibetan Plateau. *Earth and*

planetary science letters 81, 79–94.

RECHES, Z., HOEXTER, D.F. & HIRSCH, F. (1981) The structure of a monocline in the Syrian Arc system, Middle East-Surface and subsurface analysis. *Journal of Petroleum Geology* 3, 413–426.

RIBA, O. (1976) Syntectonic unconformities of the Alto Cardener, Spanish Pyrenees: A genetic interpretation. *Sedimentary Geology* 15, 213–133.

ROBERTSON, A.H.F. (1998) Mesozoic-Tertiary tectonic evolution of the easternmost Mediterranean area: integration of marine and land evidence. *Proceedings of the Ocean Drilling Program, Scientific Results, Vol. 160; Chapter 54*.

ROWLEY, D.B. & CURRIE, B.S. (2006) Palaeo-altimetry of the late Eocene to Miocene Lunpola basin, central Tibet. *Nature* 439, 677–681.

RYAN, W.B.F. & CITA, M.B. (1978) The nature and distribution of Messinian erosional surfaces—Indicators of a several-kilometer-deep Mediterranean in the Miocene. *Marine Geology* 27, 193–230.

ŞAFAK, Ü., KELLING, G., GÖKÇEN, N.S. & GÜRBÜZ, K. (2005) The mid-Cenozoic succession and evolution of the Mut basin, southern Turkey, and its regional significance. *Sedimentary Geology* 173, 121–150.

SCHILDGEN, T.F., COSENTINO, D., BOOKHAGEN, B., NIEDERMANN, S., YILDIRIM, C., ECHTLER, H., WITTMANN, H. & STRECKER, M.R. (2012) Multi-phased uplift of the southern margin of the Central Anatolian plateau, Turkey: A record of tectonic and upper mantle processes. *Earth and Planetary Science Letters* 317–318, 85–95.

SCHILDGEN, T.F., YILDIRIM, C., COSENTINO, D. & STRECKER, M.R. (2014) Linking slab break-off, Hellenic trench retreat, and uplift of the Central and Eastern Anatolian plateaus. *Earth-Science Reviews* 128, 147–168.

ŞENGÖR, A., ÖZEREN., S., GENÇ, T. & ZOR, E. (2003) East Anatolian high plateau as a mantle-supported, north-south shortened domal structure. *Geophysical research letters* 30, 1–12.

SOBEL, E.R., HILLEY, G.E. & STRECKER, M.R. (2003) Formation of internally drained contractional basins by aridity-limited bedrock incision. *Journal of Geophysical Research: Solid Earth* 108.

STERN, T.A. & HOLT, W.E. (1994) Platform subsidence behind an active subduction zone. *Nature* 368, 233–236.

STRECKER, M.R., ALONSO, R., BOOKHAGEN, B., CARRAPA, B., COUTAND, I., HAIN, M.P., HILLEY, G.E., MORTIMER, E., SCHOENBOHM, L. & SOBEL, E.R. (2009) Does the topographic distribution of the central Andean Puna Plateau result from climatic or geodynamic processes? *Geology* 37, 643–646.

TAPPONNIER, P., ZHIQIN, X., ROGER, F., MEYER, B., ARNAUD, N., WITTLINGER, G. & JINGSUI, Y. (2001) Oblique stepwise rise and growth of the Tibet plateau. *Science* 294, 1671–1677.

TINDALL, S.E. & DAVIS, G.H. (1999) Monocline development by oblique-slip fault-propagation folding: the East Kaibab monocline, Colorado Plateau, Utah. *Journal of Structural Geology*

21, 1303–1320.

ULU, Ü. (2002) Geological map of Turkey, Adana (No. 15) M. Şenel (Ed).

WALSH-KENNEDY, S., AKSU, A.E., HALL, J., HISCOTT, R.N., YALTIRAK, C. & ÇIFÇI, G. (2014) Source to sink: The development of the latest Messinian to Pliocene–Quaternary Cilicia and Adana Basins and their linkages with the onland Mut Basin, eastern Mediterranean. *Tectonophysics* 622, 1–21.

WILLETT, S.D. & SCHLUNEGGER, F. (2010) The last phase of deposition in the Swiss Molasse Basin: from foredeep to negative-alpha basin. *Basin Research* 22, 623–639.

WILLSEY, S.P., UMHOEFER, P.J. & HILLEY, G.E. (2002) Early evolution of an extensional monocline by a propagating normal fault: 3D analysis from combined field study and numerical modeling. *Journal of Structural Geology* 24, 651–669.

YETIŞ, C., KELLING, G., GÖKÇEN, S.L. & BAROZ, F. (1995) A revised stratigraphic framework for Later Cenozoic sequences in the northeastern Mediterranean region. *Geologische Rundschau: Zeitschrift fur Allgemeine Geologie* 84, 794.

YIN, A. & HARRISON, T.M. (2000) Geologic Evolution of the Himalayan-Tibetan Orogen. *Annual review of earth and planetary sciences* 28, 211–280.

Supplementary Material

Suppl. Material A: Seismic facies

Unit 1 is characterized by sub-parallel, high-frequency and medium-amplitude reflections with notable lateral continuity. Unit 1 appears in exploration wells as siliciclastic successions mostly Plio-Quaternary age (Aksu *et al.*, 2005a, 2014) correlated with the Nikosia and Mirtou formations of the Mesaoria Basin and Kyrenia Range (Fig. 2). The base of this unit is marked by the high amplitude and relatively continuous "M-reflector". This reflector corresponds to a horizon of regional significance associated with the late Messinian salinity crisis and the drop and lowstand of the Mediterranean sea level (Ryan & Cita, 1978). The M-reflector can be related with the deposition of a thick halite layer or the Messinian Erosional Surface (MES) of ~5,96 Ma (e.g., Cosentino *et al.*, 2013)(Fig. 5). These two characteristics allow us to confidently trace the Unit 1 package throughout the study area.

Unit 2 has low reflectivity and acoustically weak reflections, with short continuity and irregular geometry. The locally strong reflective yet discontinuous reflector that defines the base of Unit 2 is identified as the "N-reflector". Therefore, Unit 2 is bounded by the N-horizon at its base, if present, and by the M-reflector at its top (Fig. 5). Unit 2 is correlated with the Messinian Lower Evaporites and is thus mainly composed of halite and minor quantities of anhydrite and limestone and has an age at its base of ~5,59 Ma (Hsü *et al.*, 1973; Cosentino *et al.*, 2013; Faranda *et al.*, 2013). In the Aksu and Manavgat basins, the formations Taşlık, Eskiköy, and Gebiz are the lateral equivalents of Unit 2 (Karabıyıkoğlu *et al.*, 2000; Aksu *et al.*, 2005a). The Kalavasos and Lapatza formations are the Cyprus onland stratigraphic equivalents of Unit 2 (Aksu *et al.*, 2005a and the references therein).

Unit 3 lies immediately below the N-reflector or the M-reflector when Unit 2 is absent. Unit 3 is divided into two subunits. The upper subunit (Unit 3a) has high-amplitude, low-frequency and laterally-continuous, equally-spaced reflections. The lower subunit (Unit 3b) is characterized by discontinuous reflections with variable amplitude and frequency. The base of the Unit 3b cannot be clearly seen anywhere. The boundary between the Unit 3a and the Unit 3b is a local unconformity, marked by a non-continuous prominent reflector most clearly seen toward the margins of the basin, where

the Unit 2 evaporites are thinner. Continuity of this unconformity is often unclear and these subunits of Unit 3 cannot be extended along the seismic lines used in this study. Distinction between both subunits is shown in Fig. 6, and in a representative example in Case Line (Fig. 7).

The upper part of Unit 3 corresponds to deltaic and fluvial sediments of the Tortonian age (Aksu *et al.*, 2005a) and is correlated with the Sertavul and Köselerli formations (Eriş *et al.*, 2005; Ilgar & Nemec, 2005) of the Mut Basin. In the Kyrenia Range and Mesaoria Basin, it corresponds to the Pakhna Formation of Aksu et al. (Aksu *et al.*, 2005a). The lower subunit of Unit 3 is mostly formed by turbidite deposits of the middle Miocene age and its base may include the Aquitanian to Serravallian Karaisalı Formation (Aksu *et al.*, 2005a, 2014). It is correlated with the Mut and Derinçay formations of the Mut Basin. The particular characteristics observed for Unit 3 to the north of Line A are tentatively correlated with the Karpuzçay and Geceleme formations of the Aksu and Manavgat basins (Karabıyıkoğlu *et al.*, 2000). This subunit is further correlated with the Kythrea Group of the Kyrenia Range (Aksu *et al.*, 2005a)(Fig. 2).

Unit 4 is the acoustic basement in the study area, and is composed of a variety of units of Triassic to Oligocene age (Aksu *et al.*, 2005a).

Fig. Supplementary A. Main seismic facies identified for the seismic sections, as seen in Case Line.

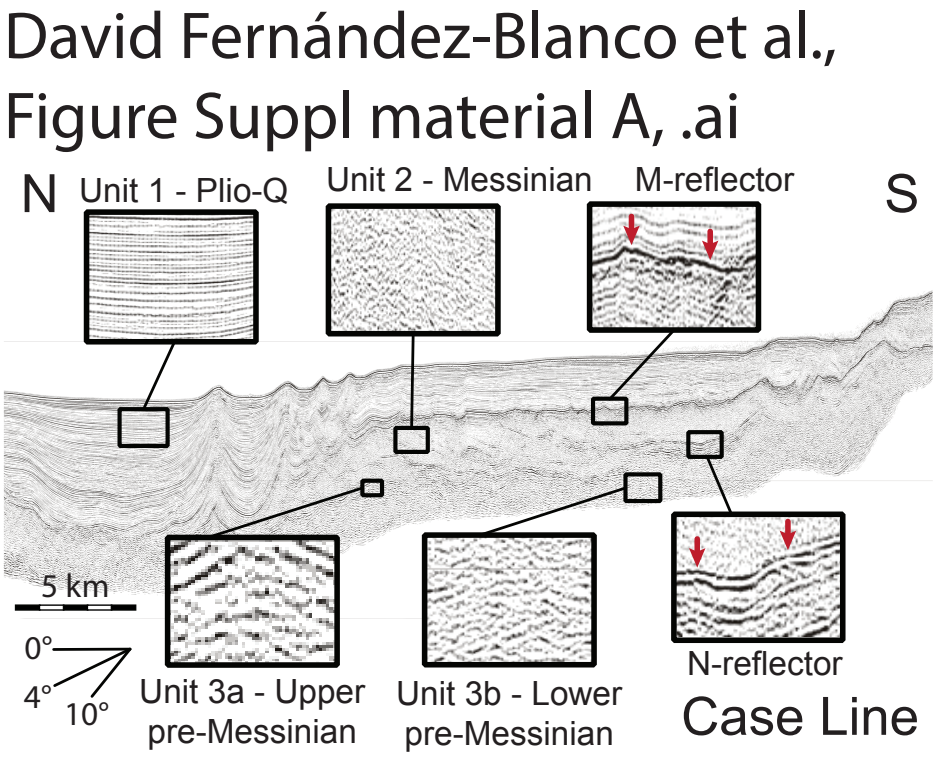

Suppl. Material B: Seismic Line Suppl. B

Line Suppl. B is located in the centre of the OCB starting south of the Turkish continental shelf (Fig. 4). In Line Suppl. B, Unit 1 (Plio-Q) forms (i) a shorter wedge (10–15 km in the horizontal) between the offshore south of Turkey and its depocentre (900 m) in the Turkish shelf break area, and (ii) a longer wedge (55–60 km in the horizontal) between the aforementioned depocentre and the offshore north of Cyprus (300 m thick) (Fig. Suppl. B). To the north of the depocentre, close to the north end of the line, several south-dipping extensional structures with little displacement appear. To the south, the long wedge marks a clear basin asymmetry, with thicknesses decreasing by two thirds from the depocentre in the Turkish shelf break to the centre of the line and slowly decreasing from there to the southern end of the line. Syntectonic wedges are seen at both sides the depocentre. Few of these syntectonic wedges are opening toward the south. However, the most relevant wedges, both in angle and in horizontal distances, open toward the north.

Unit 2 (Messinian) is thickest in the central area of Line Suppl. A, where it reaches thicknesses up to 1 km, partly in relation to the deep-rooted thrusts and salt remobilization. Unit 2 thins away both to the north and south sides of this depocentre. To the north of Line Suppl. A, Unit 2 ends underneath the Plio-Q depocentre. In the southernmost area, Unit 2 thins to values of less than 50 m and probably pinches out soon thereafter.

Unit 3 is continuous along Line Suppl. A and its base is unknown. Some top-to-the-north thrusts are seen cutting the top boundary of Unit 3 in three different regions; the deep-rooted thrusts seen in the centre of the line are the most relevant system. Toward the south of this system, a toe-of-slope thrust system in the salt-cored belt area is seen. A minor thrust is seen toward the north, where Unit 2 is thinnest.

Fig. Suppl. Material B. Original, interpreted in two-way-traveltime (TWT), traced with reflections in TWT, and depth-converted profiles of seismic reflection profile.

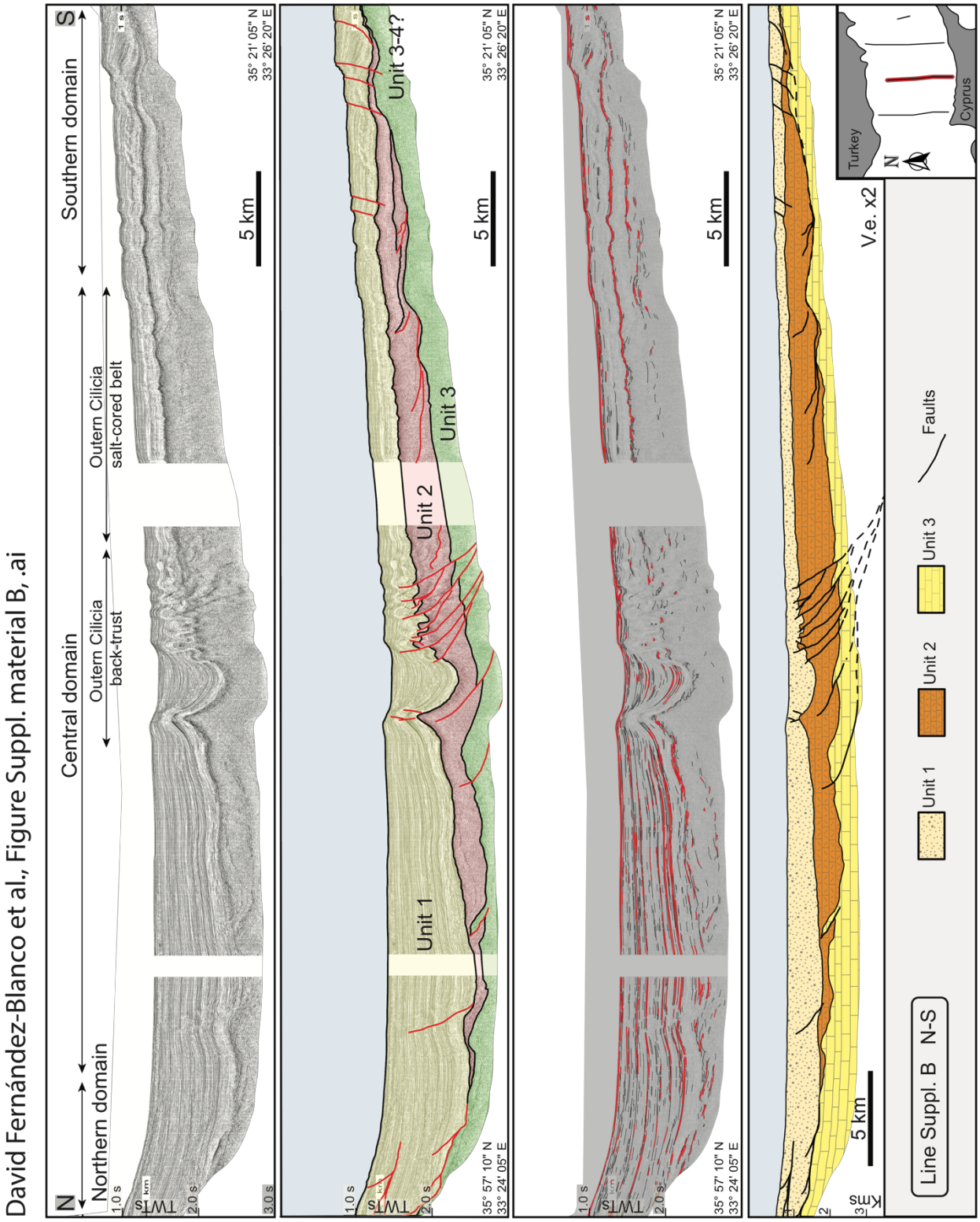
David Fernández-Blanco et al., Figure Suppl. material B, .ai
N
S
Northern domain
Central domain
Southern domain
Outern Cilicia back-trust
Outern Cilicia salt-cored belt
TWTs
1.0 s
2.0 s
3.0 s
5 km
35° 21' 05" N
33° 26' 20" E
35° 57' 10" N
33° 24' 05" E
Unit 1
Unit 2
Unit 3
Unit 3-4?
V.e. x2
Kms
Turkey
Cyprus
Line Suppl. B N-S
Faults

Suppl. Material C: Seismic Line Suppl. C

Line Suppl. C is located to the west of the study area (Fig. 4). Unit 1 (Plio-Q) shows a prominent thickening in the north from the Turkish shelf break of slope to the centre of the line, where this unit reaches its maximum thicknesses of 900–950 m. From this depocentre to north Cyprus offshore, the thicknesses of Unit 1 (Plio-Q) decrease roughly continuously to values of 250–300 m, shaping a large wedge.

Moving northward from the depocentre, Unit 1 decreases in thicknesses first gently, from 950 m to 800 m in some 10 km and then more abruptly, from 800 m to ~150 m in the Turkish shelf in ~3 km horizontal distance. The Unit 1 depocentre is bounded by opposite dipping normal faults, where both with minor displacements and some syntectonic wedges are seen. To the south end of the line, Unit 1 presents thickness variations produced by blocks tilted in association with north-dipping normal faults. These features produce southward thickening areas with syntectonic sedimentary growth in Unit 1 between the faults and the area of stair-like bathymetry.

Unit 2 (Messinian) reaches thicknesses of more than 1 km in the centre of the line. Here, the presence of several north-verging thrust tips and halokinetic structures creates the bulged upper boundary of Unit 2. North of the depocentre, the base of the unit becomes unclear due to a strong sea bed multiple. Southward of the depocentre, Unit 2 thins to 350 m or less within approx. 7 km and further thins to less than 50 m in the southernmost end of the line, probably terminating against the underlying unit soon after in that direction.

As seen in the other lines, the top of Unit 3 (pre-Messinian Miocene) is transected in the centre of Line Suppl. C by a top-to-the-north deep-rooted thrust system. Since the Unit 3 bottom is unknown, thickness analysis was not performed.

Fig. Suppl. Material C. Original, interpreted in two-way-traveltime (TWT), traced with reflections in TWT, and depth-converted profiles of seismic reflection profile Suppl. Material C.

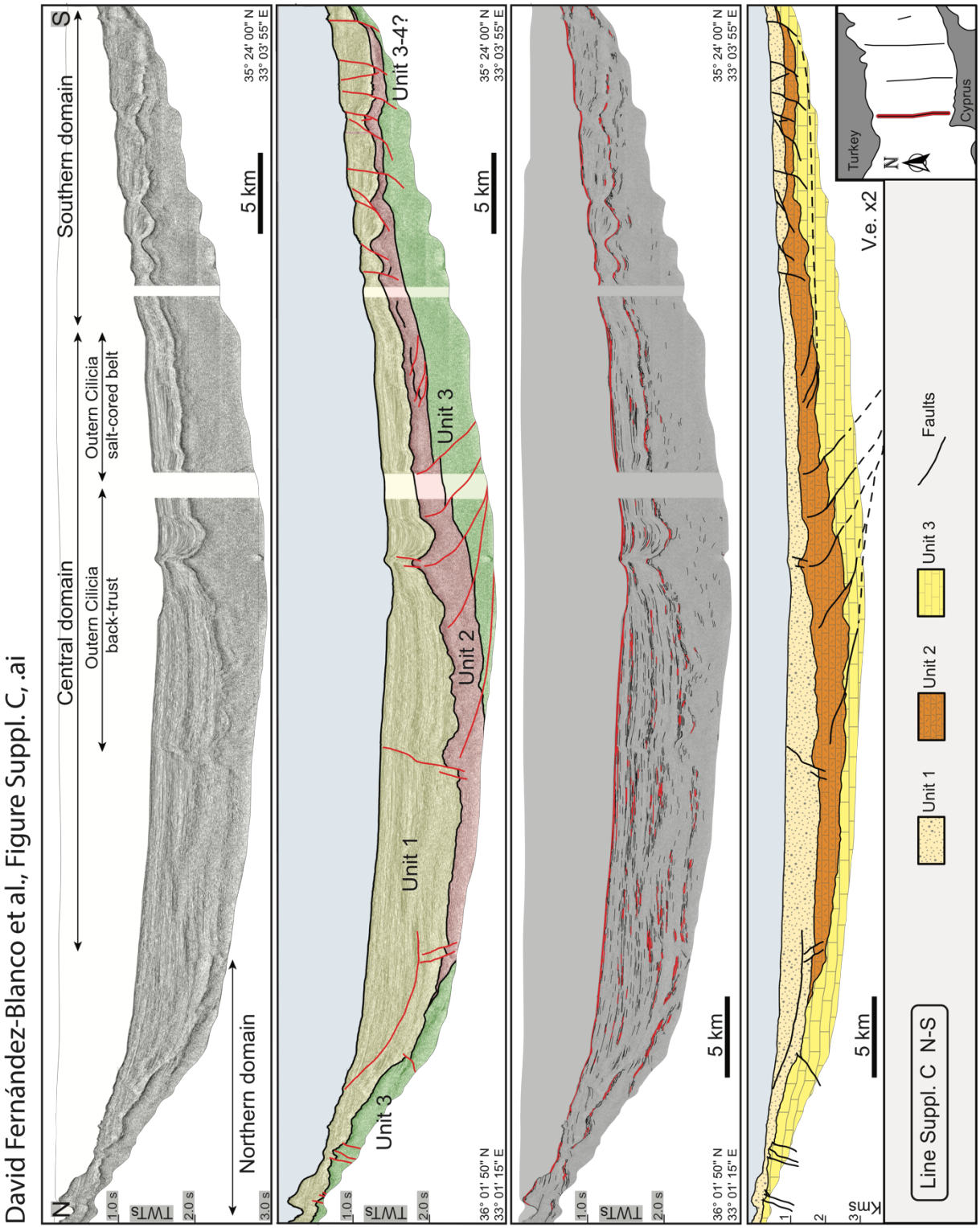
David Fernández-Blanco et al., Figure Suppl. C, .ai
N
S
Southern domain
Central domain
Outern Cilicia back-trust
Outern Cilicia salt-cored belt
Northern domain
TWTs
1.0 s
2.0 s
3.0 s
5 km
35° 24' 00" N
33° 03' 55" E
36° 01' 50" N
33° 01' 15" E
Unit 1
Unit 2
Unit 3
Unit 3-4?
V.e. x2
kms
Turkey
Cyprus
Faults
Line Suppl. C N-S

Suppl. Material D: Kinematics in the central OCB

Unit 1 (latest most Messinian - Recent) varies in thickness at the front of the tips of the Central OCB main thrust (Figs. 6 and Suppl. D). The three foremost slivers of the deep-rooted north-verging thrust system have a clear expression in the overlying sequence that implies the structure is of very young age or reactivated recently. We distinguish two subpackages within Unit 1 on the basis of thicknesses variations between laterally continuous reflections (Fig. 7-D). Upper subunit thicknesses are roughly continuous with minor thinning on top of the thrust crests of the thrusts. Lower subunit thicknesses vary relevantly, having considerably thinner sequences at the thrust crests than to their sides. These thickness differences are more obvious toward the base of the unit (Fig. 7-D). Variable thicknesses between the crest and valleys of the frontal low-dipping thrust to the north lead to progressive unconformities. These progressive unconformities record structural development and growth during the mid-upper Unit 1, and apparent quiescence during deposition of the unit upper section (Fig. 7-D). This and the relatively thick Unit 1 sequence on top of the anticline crests are clear signs of contraction. The relative shallowness of the southern half of the OCB is caused by these top-to-the-north deep-rooted thrusts and associated fold structures (Fig. Suppl.D-D). We consider this set of imbricated thrusts to be a back-thrust fault system that coalesces in depth with the south-verging structures of the Kyrenia Range.

Fig. Suppl. D. Inset A is the seismic image in time with traced reflections showing the angular relationships of the Plio-Q in the center of the OCB. Three packages are seen as a function of their angular relationship with the underlying growing structure, numbered from oldest to youngest. Representative dips of reflections in each unit units are shown in blue. Inset B is the conceptual evolution of the central sector of the basin derived from the analysis of the seismic reflections.

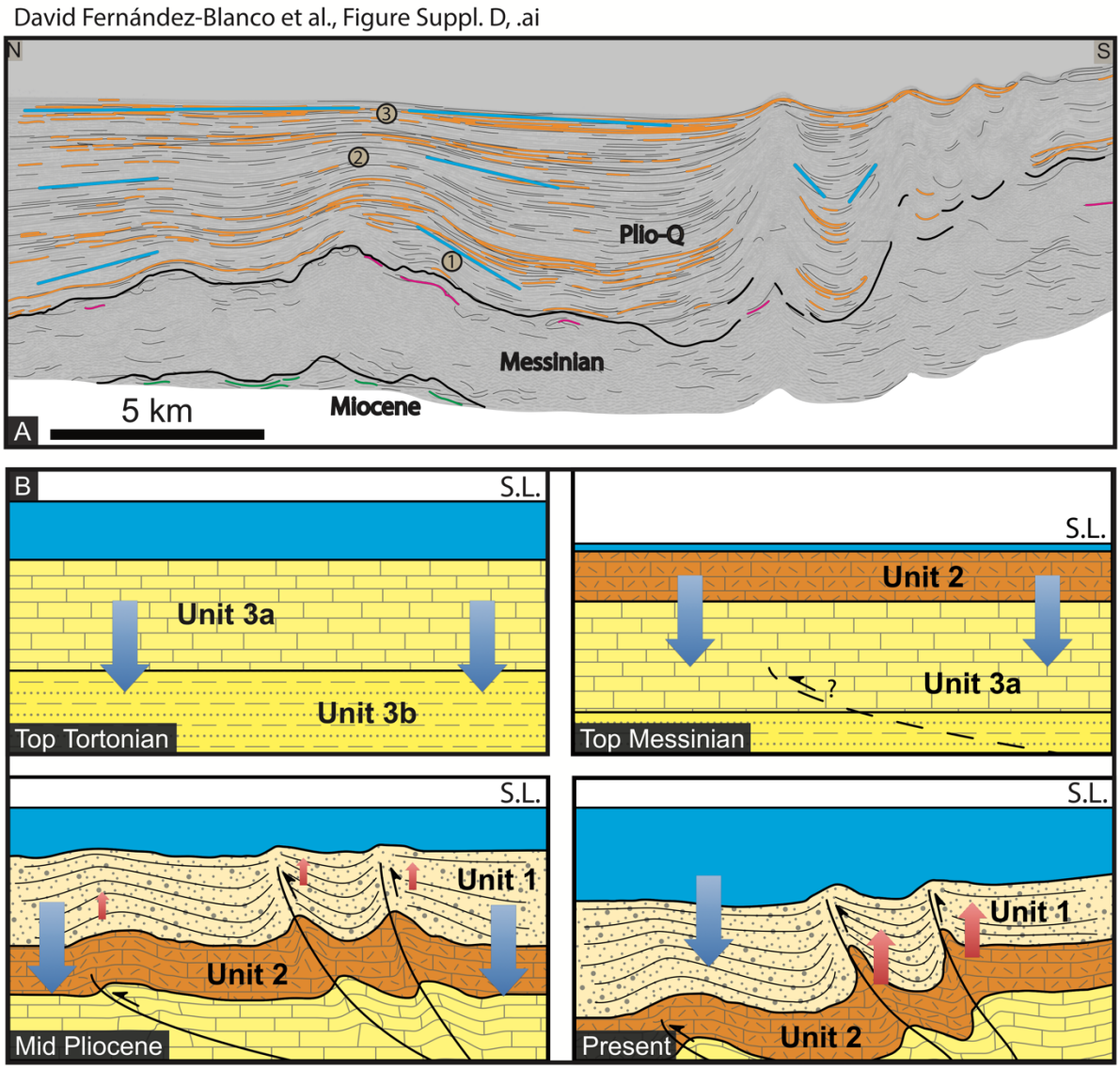

Suppl. Material E: Kinematics in the southern OCB

An extensional system transects Unit 1 on the Cyprus shelf, and further north, a north-verging thrust system gently dipping south (α-reflectors of Aksu *et al.*, 2005a) lie within Unit 2 (Fig. 6 & Suppl. E). While reflections showing synsedimentary growth in the extensional fault hanging-walls set faulting onset to lower-to-middle Unit 1 (latest Messinian-Early Pliocene), the sea floor step-like bathymetry indicates that motion may still be active in Recent times. The main slip surface of the extensional system is probably kinematically linked with the main detachment level of the thrust system in a toe-of-slope conjugate system. This indicates that both sets of structures developed jointly due to gravity, most probably through the slope instability of Messinian evaporites (Fig. Suppl. E). We consider this structure to be a kinematic response of a perched basin margin to uplift (further south) in relation to the south-verging structures forming the Kyrenia Range.

Fig. Suppl. material E. Inset A corresponds to a seismic image in time with traced reflections showing the angular relationships seen in the Plio-Q Unit in the southern margin of the OCB. Representative dips of reflections in each unit units are shown in blue. Inset B is the conceptual evolution of the south margin of the OCB, as derived from the analysis of seismic reflections in the northern boundary of the OCB.